Article

Cell Reports

Butyrate Protects Mice from *Clostridium difficile*-Induced Colitis through an HIF-1-Dependent Mechanism

Graphical Abstract

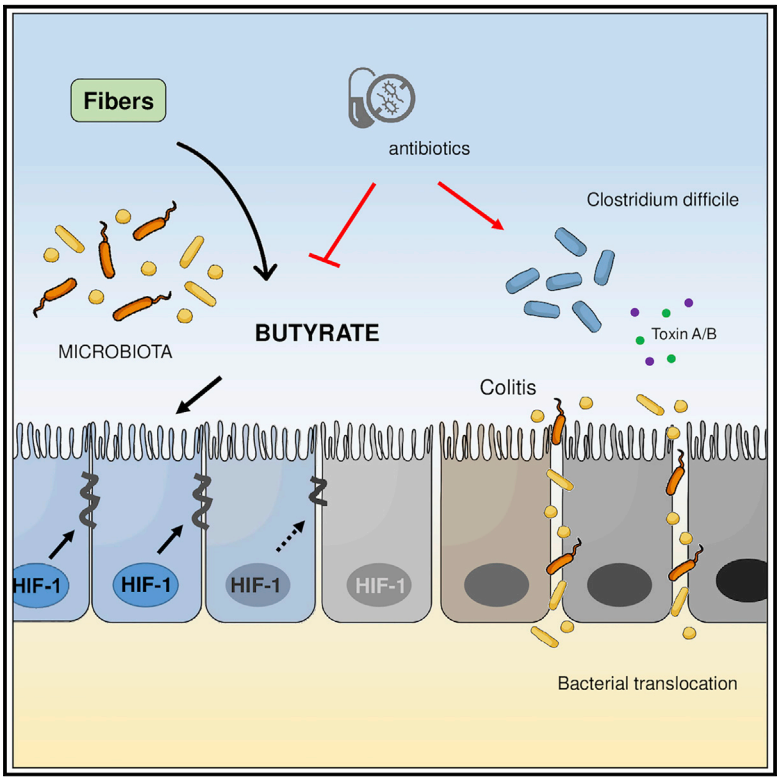

Highlights

- Butyrate mitigates the pathogenicity of colitis induced by *Clostridium difficile*
- Butyrate increases expression of tight junctions in epithelial cells
- Butyrate reduces intestinal inflammation and bacterial translocation
- HIF-1 stabilization is necessary to the protection induced by butyrate

Authors

José Luís Fachi,
Jaqueline de Souza Felipe,
Laís Passariello Pral, ...,
Alessandro dos Santos Farias,
Patrick Varga-Weisz,
Marco Aurélio Ramirez Vinolo

Correspondence

mvinolo@unicamp.br

In Brief

Fachi et al. demonstrate that butyrate is able to protect the intestinal epithelium from the damage caused by *Clostridium difficile* toxins by stabilizing HIF-1 and increasing tight junctions, which reduces intestinal epithelial permeability, thus inhibiting intestinal inflammation and bacterial translocation.

Fachi et al., 2019, Cell Reports *27*, 750–761
April 16, 2019
https://doi.org/10.1016/j.celrep.2019.03.054

CellPress

OPEN ACCESS
CellPress

Cell Reports
Article

Butyrate Protects Mice from *Clostridium difficile*-Induced Colitis through an HIF-1-Dependent Mechanism

José Luís Fachi,[1] Jaqueline de Souza Felipe,[1] Laís Passariello Pral,[1] Bruna Karadi da Silva,[1] Renan Oliveira Corrêa,[1] Mirella Cristiny Pereira de Andrade,[1] Denise Morais da Fonseca,[2] Paulo José Basso,[2] Niels Olsen Saraiva Câmara,[2] Éricka Lorenna de Sales e Souza,[3] Flaviano dos Santos Martins,[3] Suzana Eiko Sato Guima,[4] Andrew Maltez Thomas,[4] João Carlos Setubal,[4,5] Yuli Thamires Magalhães,[4] Fábio Luis Forti,[4] Thamiris Candreva,[6] Hosana Gomes Rodrigues,[6] Marcelo Bispo de Jesus,[7] Sílvio Roberto Consonni,[8] Alessandro dos Santos Farias,[9] Patrick Varga-Weisz,[10,11] and Marco Aurélio Ramirez Vinolo[1,12,*]

[1]Laboratory of Immunoinflammation, Department of Genetics, Evolution, Microbiology, and Immunology, Institute of Biology, University of Campinas, Campinas, SP 13083-862, Brazil
[2]Department of Immunology, Institute of Biomedical Sciences, University of São Paulo, São Paulo, SP 05508-900, Brazil
[3]Laboratory of Biotherapeutics Agents, Department of Microbiology, Institute of Biological Sciences, Federal University of Minas Gerais, Belo Horizonte, MG 31270-901, Brazil
[4]Department of Biochemistry, Institute of Chemistry, University of São Paulo, São Paulo, SP 05508-000, Brazil
[5]Biocomplexity Institute, Virginia Polytechnic Institute, Blacksburg, VA 24061, USA
[6]Laboratory of Nutrients and Tissue Repair, School of Applied Sciences, University of Campinas, Limeira, SP 13484-350, Brazil
[7]Nano-Cell Interactions Lab, Department of Biochemistry and Tissue Biology, Institute of Biology, University of Campinas, Campinas, SP 13083-862, Brazil
[8]Laboratory of Citochemistry and Immunocitochemistry, Department of Biochemistry and Tissue Biology, Institute of Biology, University of Campinas, Campinas, SP 13083-862, Brazil
[9]Laboratory of Neuroimmunology, Department of Genetics, Evolution Microbiology, and Immunology, Institute of Biology, University of Campinas, Campinas, SP 13083-862, Brazil
[10]Nuclear Dynamics Programme, Babraham Institute, Cambridge CB22 3AT, UK
[11]School of Biological Sciences, University of Essex, Colchester CO4 3SQ, UK
[12]Lead Contact
*Correspondence: mvinolo@unicamp.br
https://doi.org/10.1016/j.celrep.2019.03.054

SUMMARY

Antibiotic-induced dysbiosis is a key factor predisposing intestinal infection by *Clostridium difficile*. Here, we show that interventions that restore butyrate intestinal levels mitigate clinical and pathological features of *C. difficile*-induced colitis. Butyrate has no effect on *C. difficile* colonization or toxin production. However, it attenuates intestinal inflammation and improves intestinal barrier function in infected mice, as shown by reduced intestinal epithelial permeability and bacterial translocation, effects associated with the increased expression of components of intestinal epithelial cell tight junctions. Activation of the transcription factor HIF-1 in intestinal epithelial cells exerts a protective effect in *C. difficile*-induced colitis, and it is required for butyrate effects. We conclude that butyrate protects intestinal epithelial cells from damage caused by *C. difficile* toxins via the stabilization of HIF-1, mitigating local inflammatory response and systemic consequences of the infection.

INTRODUCTION

Clostridium difficile is a Gram-positive anaerobic bacillus that forms spores, conferring resistance to environmental factors and allowing persistence for several months on surfaces and food and in water. This bacterium is a common cause of intestinal infection, which mainly affects hospitalized patients, and is recognized as a serious public health problem (Martin et al., 2016). A continuous increase in the incidence, morbidity, and mortality of patients infected with *C. difficile* has been seen in recent decades (Martin et al., 2016). The development of clinical disease most commonly occurs after the ingestion of spores by a susceptible host. A major risk factor for *C. difficile* infection (CDI) is antibiotic use, which induces changes in indigenous intestinal microbiota, impairing resistance (Chen et al., 2008; Lamont and Hajishengallis, 2015; Rodriguez et al., 2015). Additional risk factors include age, immunological state, and comorbidities (Lamont and Hajishengallis, 2015; Rea et al., 2011).

CDI presents symptoms ranging from mild to moderate non-bloody diarrhea and intestinal discomfort to severe forms with intense diarrhea and abdominal pain, pseudomembranous colitis, and more serious complications such as toxic megacolon, peritonitis, respiratory distress, sepsis, and death (Johanesen et al., 2015; Lamont and Hajishengallis, 2015). These symptoms are

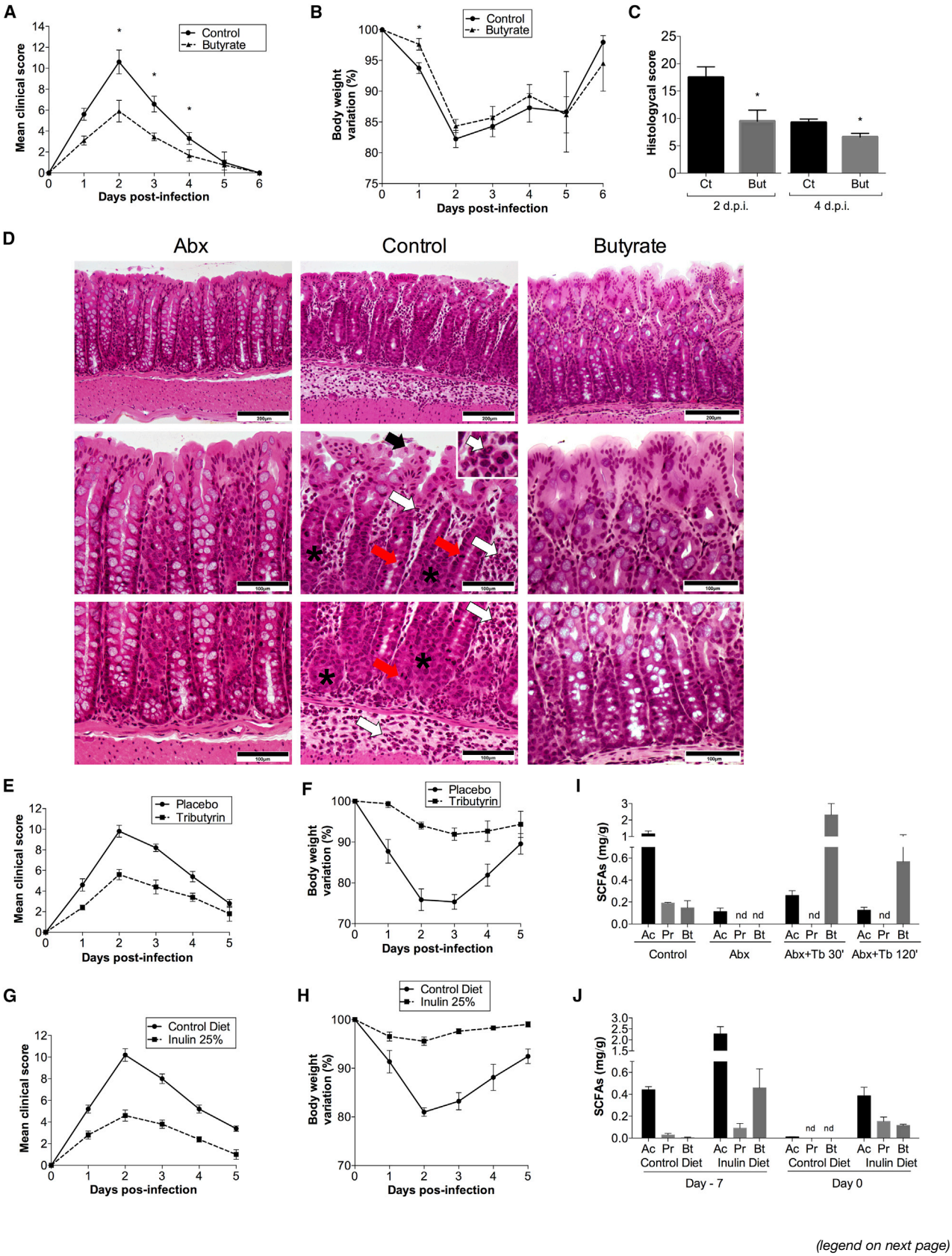

(legend on next page)

associated with the actions of the two major *C. difficile* virulence factors, toxin A (TcdA) and toxin B (TcdB) (Kuehne et al., 2010; Rodriguez et al., 2015). These toxins glycosylate Rho family proteins, keeping them in an inactive form and thus affecting downstream pathways, including cytoskeleton organization. The cytoskeletal effects lead to the disruption of the cellular actin structure and the death of intestinal epithelial cells (IECs), resulting in the loss of barrier function and, consequently, a profound inflammatory response (Cohen et al., 2011; Rodriguez et al., 2015).

The intestinal microbiota confers resistance against CDI. Studies conducted in humans and mice have shown that gut microbiota prevent intestinal colonization by *C. difficile* (Buffie et al., 2015; Stecher and Hardt, 2008; Theriot et al., 2014; van Nood et al., 2013) and that fecal microbiota transplant is an effective treatment for recurrent CDI (van Nood et al., 2013). The transference of specific components from microbiota, such as secondary bile salt metabolites, has been found to confer resistance against CDI in mice (Buffie et al., 2015). However, the mechanisms involved in microbiota protection are not well understood.

A major link between microbiota and host cells is the production of short-chain fatty acids (SCFAs) through bacterial metabolism. These molecules (mainly acetate, propionate, and butyrate) are released into the intestinal lumen from fiber metabolization and absorbed by IECs. SCFAs have several immunomodulatory effects (Corrêa-Oliveira et al., 2016). Strategies that increase their intestinal concentrations are effective in reducing tissue damage and increasing immune system effector mechanisms. In this way, SCFAs improve the host response to inflammatory and infectious stimuli (Galvão et al., 2018; Kim et al., 2013; Maslowski et al., 2009; Vieira et al., 2017). Recent reports have noted that SCFA-producing bacteria are depleted and that SCFA concentrations are significantly reduced in the intestines of CDI patients (Antharam et al., 2013). In addition, CDI-susceptible mice have lower intestinal concentrations of SCFAs compared to CDI-resistant mice (Theriot et al., 2014). Here, we aimed to investigate the impact of administering the SCFA butyrate on an acute CDI mouse model.

RESULTS

Microbiota Changes after Antibiotic Treatment Affect SCFA Production

Samples were collected from mice that were either resistant (before antibiotic treatment) or susceptible to *C. difficile* infection (day 0). In addition, we collected samples from mice recovering from antibiotic treatment (day 6). A reduction in fecal bacterial load in CDI-susceptible mice compared to the other groups was observed (Figure S1E). After antibiotic treatment, mice showed a reduction in microbial diversity, found by comparing rarefaction curves with those from mice before antibiotic treatment. Microbial diversity partially recovered 7 days after clindamycin treatment (not shown). At the phylum level, we observed a reduction in Bacteroidetes (e.g., *Barnesiella*, *Alistipes*) and a less evident reduction in Firmicutes (e.g., *Clostridium* cluster XIVa, *Lachnospiraceae*) in mice after antibiotic treatment. A relative increment of Proteobacteria (e.g., components of the *Enterobacteriaceae* family, *Parasutterella*) and Verrucomicrobia (e.g., *Akkermansia*) was seen in antibiotic-treated mice (Figures S1A–S1D). These effects were accompanied by marked changes in SCFA production in the colon (Figure S1F). Five days after clindamycin administration (day 4), concentrations of SCFAs (apart from butyrate) were similar to those before antibiotic treatment (Figure S1F). Thus, butyrate production was persistently compromised, even though microbiota composition partially recovered after antibiotic treatment.

Oral Administration of Butyrate, Tributyrin, and Inulin Diet Protects against CDI

The addition of 150 mM butyrate to the drinking water of mice resulted in a protective effect against CDI. An improvement in clinical and colon histological scores was observed in butyrate-treated mice (Figures 1A–1C). A histological examination of the colon at the peak of the infection (day 2) revealed epithelial damage, moderate depletion of goblet cells, and evident mitosis at the intestinal crypts. Extensive infiltration of inflammatory cells (mainly granulocyte neutrophils) was observed in colonic lamina propria (LP) and submucosa in infected mice as compared to uninfected mice (Figure 1D). The changes were less evident on day 4 (Figure 1C). Butyrate-treated mice showed improved parameters, particularly epithelial ulceration and accumulation of cells in the LP and submucosa area (Figure 1D), at the peak of the infection. Administration of a pro-drug of butyrate, tributyrin, or an inulin-rich diet had the same effect on CDI, as both conditions resulted in protection of the mice (Figures 1E–1H). Both strategies increased butyrate intestinal concentrations in antibiotic-treated mice (Figures 1I and 1J). The inulin-rich diet also increased acetate and propionate concentrations, which may be relevant for the effect of the diet (Figure 1J).

Figure 1. Oral Administration of Butyrate, Tributyrin, and Inulin Diets Protects Mice against CDI

Mice were treated with antibiotic mixture for 4 days and then received a single dose of clindamycin. After 1 day, mice were infected with *C. difficile* (day 0). Mice received 150 mM butyrate during the entire protocol.

(A and B) Mice were clinically monitored (A) and weighed (B) until day 6 after infection (n = 10).

(C) Histological score of mice ± treatment with butyrate (n = 5).

(D) Representative colon histological sections of antibiotic (Abx)-treated mice and *C. difficile*-infected mice at day 2 post-infection ± butyrate treatment. Arrows and asterisks in the sections indicate major histopathological differences between groups: polymorphonuclear infiltration of the LP and submucosa (white arrows), epithelial damage (black arrow), reduction of goblet cells (asterisks), and hyperplasia (red arrows). Upper scale bar: 100 μm, lower scale bar: 50 μm.

(E–J) Mice treated with placebo (PBS) or tributyrin and infected with *C. difficile* were clinically monitored (E) and weighed (F) until day 5 after infection (n = 5). Mice treated with control or inulin-supplemented diet for 7 days and infected. They were clinically monitored (G) and weighed (H) until day 5 post-infection (n = 5). Results are means ± SEMs. Measurement of SCFA concentrations in the colon content of Abx-treated mice supplemented with tributyrin (I). Samples were collected after 30 or 120 min of tributyrin administration. Results are presented as means ± SEMs (n = 2–3). Measurement of SCFA concentrations in the fecal samples of mice treated with control or inulin-supplemented diet (J). Samples were collected before Abx treatment (day −7) and at the infection day (day 0). Results are presented as means ± SEMs (n = 5). nd, not detected.

*$p < 0.05$ compared to control. See also Figure S1.

Butyrate Does Not Interfere in *C. difficile* Colonization or Toxin Production

Since a recent study found that the consumption of a fiber-enriched diet modified gut microbiota, *C. difficile* burdens, and toxin production (Hryckowian et al., 2018), we tested the effect of butyrate on the microbiota composition of infected mice, *C. difficile* colonization, and toxin production. The administration of butyrate affected the overall microbial community structure before infection (day 0, $p = 0.01$; analysis of similarities), but it did not affect specific phyla/genera ($q > 0.05$) or bacterial richness (Figures S2A–S2C). Butyrate still had a protective effect in germ-free mice infected with *C. difficile*, indicating that at least part of its effect is independent of microbiota changes (Figure S2D).

Next, we incubated bacteria with different butyrate concentrations and found that this limited growth of *C. difficile* only at a high concentration (50 mM) (Figure S2E) and that 10 and 50 mM butyrate increased the production of TcdA and TcdB (Figure S2F) due to cytotoxic and sporulation effects. However, butyrate treatment did not affect *C. difficile* colonization or toxin production in specific pathogen-free or germ-free mice (Figures S2G–S2J), indicating that the beneficial effects did not involve a direct effect on *C. difficile* burdens or toxin production. Tributyrin treatment also did not affect *C. difficile* colonization in mice (data not shown).

Intestinal Inflammation Is Attenuated by Butyrate, but It Is Not Required for Protective Effect in CDI

Consistent with the findings above, butyrate administration reduced the levels of pro-inflammatory cytokines (interleukin 6 [IL-6], IL-1β, and chemokine ligand 1 [Cxcl-1]) and increased the anti-inflammatory cytokine IL-10 in the colon at the peak of infection (Figure 2A). We next found that butyrate treatment increased the expression of *Il-10* and *Foxp-3* transcripts in colon and mesenteric lymph nodes (mLNs) (Figures 2B and 2C), accompanied by changes in the expression of several cytokines in these tissues (Figures S3A and S3B) (indicating an effect on regulatory T [Treg] cells). No effect of butyrate on cytokine production in antibiotic-treated mice was observed (Figure S3C).

Previous studies showed that butyrate increases Treg numbers and function in the colon (Arpaia et al., 2013; Smith et al., 2013). Our results in Foxp-3 GFP mice treated with antibiotics and supplemented with butyrate corroborated these data (Figure 2D). We also found increased $CD103^+$ dendritic cells in mLNs of mice treated with antibiotics and supplemented with butyrate compared to mice receiving antibiotic treatment only (Figures 2E and S3H–S3J). To gain insight into the role of T cells and the anti-inflammatory cytokine IL-10, we repeated the experiment in Rag1- and IL-10-deficient mice ($Rag1^{-/-}$ and $Il10^{-/-}$). In both strains, butyrate protected against CDI (Figures 2F, 2G, S4A, and S4B), indicating that part of the effect of butyrate in this model is independent of the actions on T cells or IL-10.

Butyrate Reduces Intestinal Permeability and Microbial Translocation

As bacterial translocation after CDI damage in the intestinal barrier causes systemic inflammatory response and contributes to disease severity (Hasegawa et al., 2014), we tested the effect of butyrate on intestinal permeability in infected mice. Analyses of bacteria translocation to peripheral organs (livers, spleens, and mLNs) on day 2 after infection showed a high proportion of mice with bacteria present in these organs (Figures 3A–3D and S4D). Oral treatment with butyrate significantly reduced the colony-forming units (CFUs) in the liver (Figure 3A). We also found a higher proportion of livers that were positive for bacteria in control mice compared to those from butyrate-treated mice (54% versus 23% and 69% versus 54% under anaerobic and aerobic conditions, respectively). A similar pattern was observed for the spleen (Figures S4C and S4D). These results were confirmed by bacterial 16S rDNA qPCR (Figure 3D). Fluorescence *in situ* hybridization (FISH) analysis showed that butyrate-treated mice had a lower depletion of mucus and translocation of bacteria (Figure 3F). We also observed increased space between microbiota and IECs (Figure 3F). Next, we tested the effect of butyrate on intestinal epithelial permeability in CDI mice by fluorescein isothiocyanate (FITC)-dextran gavage on day 2 post-infection, with a measurement of translocation 4 h later. We consistently found a significant reduction in FITC-dextran translocation in butyrate-treated mice (Figure 3E). This was also observed in *Rag-1*-deficient mice (Figure S4B). Intestinal permeability, measured by bacteria and FITC-dextran translocation, was not different in uninfected mice (antibiotic ± butyrate).

We found that butyrate treatment of infected mice increased the expression of genes associated with paracellular junction proteins, including *Claudin-1* and *Occludin* (Figure S4E). The idea that butyrate improved the intestinal barrier was also corroborated by data obtained by immunostaining claudin-1, an important protein for maintaining epithelial integrity. This protein was increased in butyrate-treated mice as compared to mice receiving antibiotic treatment only (Figures 3G and 3H). These results indicate that butyrate acts directly on the intestinal barrier, and this may be relevant for the protection observed in the CDI model.

Activation of HIF-1 in IECs Is Required for Butyrate Effects

To investigate the direct effects of butyrate on IECs, we used HCT116 cells. The cytotoxic effect of *C. difficile* supernatant (containing high concentrations of TcdA/TcdB) was tested *in vitro*. Colon cells exposed to *C. difficile* supernatant showed reduced transepithelial electrical resistance (TEER), and butyrate partly prevented this effect (Figure 4A). Butyrate also attenuated the impact of *C. difficile* supernatant on viability and monolayer reduction (Figures 4B, 4C, and S4F).

Recent studies showed that butyrate stabilizes hypoxia-inducible factor 1α (HIF-1α) in IECs, an effect that is relevant to intestinal barrier integrity (Kelly et al., 2015; Rivera-Chávez et al., 2016). The expression of HIF-1 targets and genes related to the paracellular junction was higher in cells incubated with butyrate compared to controls (Figure 4D). In agreement with the idea that HIF-1 stabilization has a role in the effects, we found that HCT116 cells incubated with the HIF stabilizer BAY 85-3934 were more resistant to *C. difficile* supernatant-induced death (Figure 4E).

Oral administration of butyrate to infected mice increased the levels of HIF-1α mRNA and its target genes, including

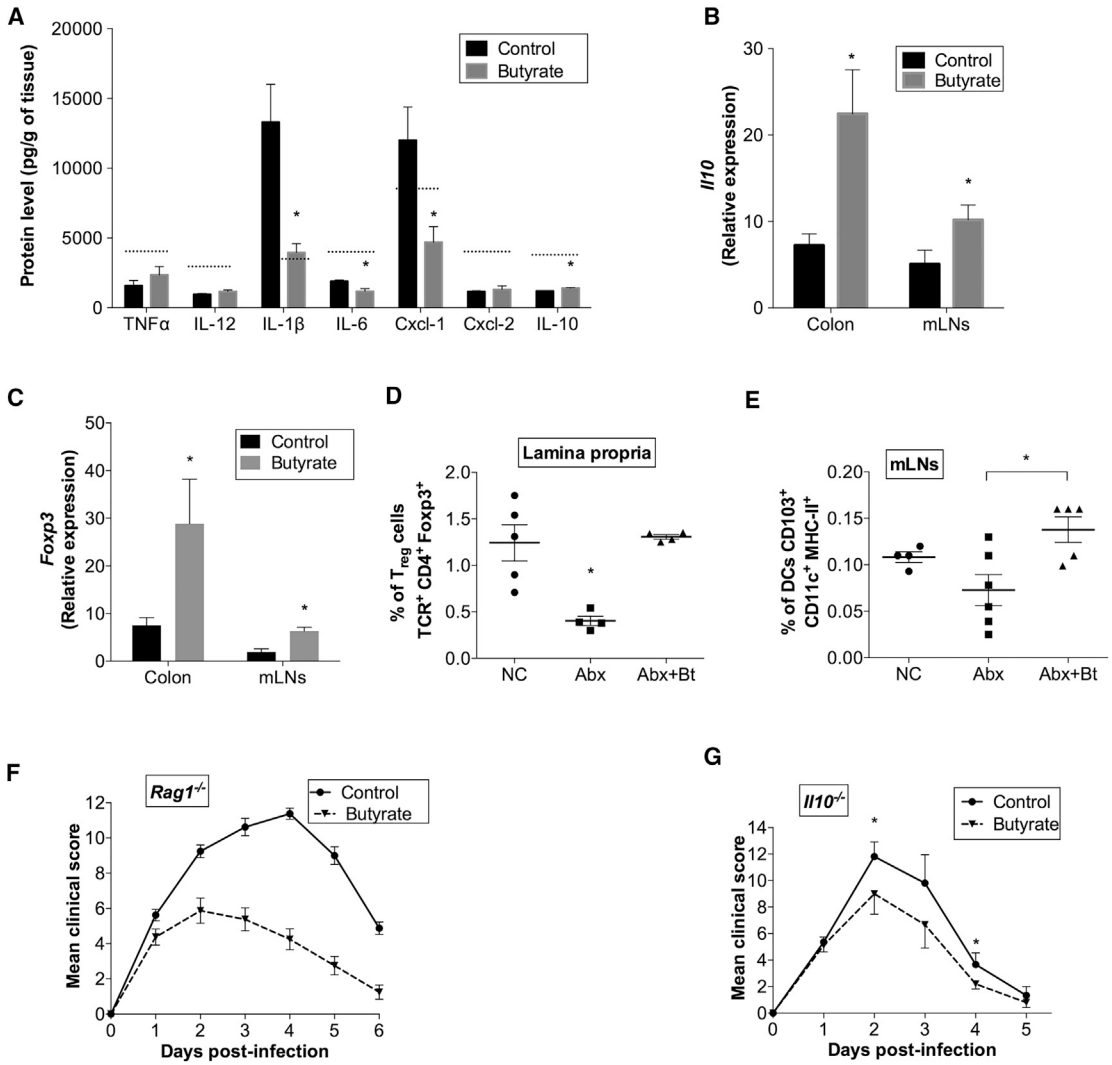

Figure 2. Intestinal Inflammation Is Attenuated by Butyrate, but It Is Not Required for Protective Effect in CDI

(A) Quantification of cytokines in the colons of *C. difficile*-infected mice ± butyrate treatment. Results were normalized by tissue weight (n = 4–5). Dashed line indicates the mean value obtained with samples from non-infected mice.

(B and C) qPCR analysis of *Il10* (B) and *Foxp3* (C) transcripts in colons and mLNs (n = 8). Results were normalized by values obtained with samples from non-infected mice and are presented as means ± SEMs.

(D) Percentage of Treg cells ($TCRb^+CD4^+FoxP3^+$) in colonic LP.

(E) Percentage of dendritic cells ($CD11c^+MHCII^+CD103^+$) in mLNs. NC, control mice with no treatment; Abx, mice treated with antibiotics for 4 days; Abx + Bt, mice that received antibiotics and 150 mM butyrate for 4 days (n = 4–6).

(F) Clinical score of *Rag1*-deficient mice infected with *C. difficile* ± butyrate (n = 8).

(G) Clinical score of *Il10*-deficient mice infected with *C. difficile* ± butyrate (n = 9–10).

*$p < 0.05$ compared to control.

cathelicidin antimicrobial peptide (*Camp*), vascular endothelial growth factor *(Vegfa),* and trefoil factor 3 (*Tff3*) in the colons of infected mice (Figures 5A and 5B). Corroborating these data, we observed increased HIF-1α in the colon after butyrate administration to oxygen-dependent degradation domain (ODD)-luciferase mice (Figure 5C). We next tested a potential role for HIF-1 in the butyrate effect on CDI using $Hif1a^{\Delta IEC}$. Co-housed villin-Cre^+ ($Hif1a^{\Delta IEC}$, knockout [KO]) and Cre^- ($Hif1a^{f/f}$, wild type [WT]) littermates from $Hif1a^{flox/flox}$ × villin-Cre crosses were used in the experiments. Using these mice, we found that the effect of butyrate on intestinal permeability was lost, as shown by the absence of differences in FITC-dextran translocation between HIF-1-deficient mice ± treatment with butyrate (Figure 5D). This was corroborated by the finding that butyrate-treated deficient mice showed no changes in the translocation of bacteria compared to their controls (Figure 5E). $Hif1a^{\Delta IEC}$-infected mice presented a poorer clinical score compared to their controls, and butyrate protection was abrogated (Figures 5F and 5G). These experiments were repeated using von Hippel-Lindau tumor suppressor (*Vhl*)-deficient mice ($Vhl^{\Delta IEC}$ mice). The protein

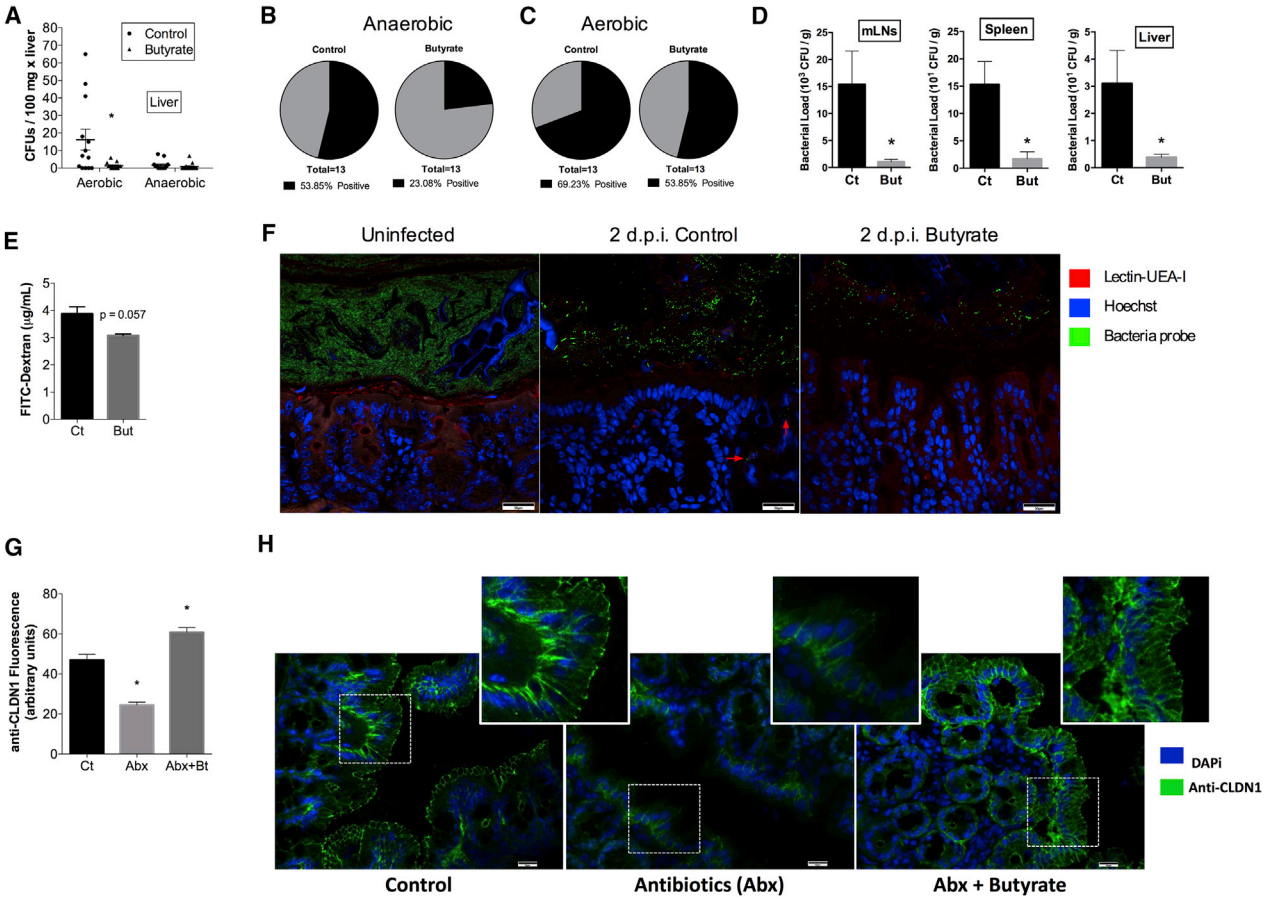

Figure 3. Butyrate Reduces Intestinal Permeability and Microbial Translocation

(A) Analysis of bacterial translocation by plating the livers of mice treated with antibiotics and infected with *C. difficile*. Samples were collected 2 days post-infection, plated, and incubated for 4 days at 37°C (n = 13).

(B and C) Percentage of mice positive for bacterial growth in anaerobic (B) and aerobic (C) conditions (n = 13). Black: positive bacterial translocation, gray: negative for bacterial translocation.

(D) qPCR analysis of relative bacterial load translocated to mLNs, spleens, and livers of mice infected with *C. difficile* (n = 5–7).

(E) Analysis of intestinal permeability using FITC-dextran received on day 2 of infection. Sera were collected after 4 h (n = 3–4).

(F) Confocal microscopy analysis of mucus, microbiota, and mucosal integrity (n = 6). Arrows indicate translocated bacteria. Scale bars represent 50 μm.

(G and H) Immunofluorescence analysis of epithelial junction for detection of claudin-1 in colon (n = 4). Quantification of fluorescence (G) and representative immunofluorescence images (H) showing claudin-1 in colon sections of control, antibiotic, and antibiotic+butyrate treated mice. Scale bars: 15 μm.

*$p < 0.05$ compared to control. See also Figures S3 and S4.

encoded by this gene plays a major role in the ubiquitination and degradation of HIF-α subunit of the hypoxia-inducible factor. Therefore, the deletion of *Vhl* results in the constitutive activation of HIF. Further corroborating the idea that butyrate acted through HIF-1, we found that the treatment of $Vhl^{\Delta IEC}$ mice did not have a significant effect on clinical parameters after infection with *C. difficile* (Figures S5A and S5B).

Histologically, we observed that butyrate-treated $Hif1a^{\Delta IEC}$ presented increased numbers of infiltrating cells in the colonic LP and submucosa compared to their controls treated with butyrate (not shown). We next isolated IECs from butyrate-treated $Hif1a^{\Delta IEC}$ and their controls (WT) and compared their transcriptomes to identify the possible mechanisms behind the increased susceptibility to CDI. We observed that in the absence of HIF-1 signaling, 620 genes were downregulated and 460 were upregulated ($p < 0.05$; Figure 5H). To explore the functional annotation and pathway enrichments of DEGs (differentially expressed genes), we used DAVID Bioinformatics resources. DEGs downregulated in $Hif1a^{\Delta IEC}$ were associated with biological processes such as the immune response to microorganisms (virus and Gram-positive bacteria) and the cellular response to type I and type II interferons. In the Kyoto Encyclopedia of Genes and Genomes (KEGG) pathways analysis, terms associated with the response to microorganisms such as phagosome, pattern recognition receptors signaling, antigen processing and presentation, and the maintenance of the epithelial barrier (i.e., cell adhesion molecules) were downregulated in $Hif\text{-}1a^{\Delta IEC}$. However, DEGs upregulated in $Hif\text{-}1a^{\Delta IEC}$ were associated with metabolism, mainly lipid metabolism (Figure 5I). These results indicate that HIF-1 activation by butyrate reduces the intestinal epithelium damage caused by CDI and improves the immune response against commensals, reducing their translocation to other tissues.

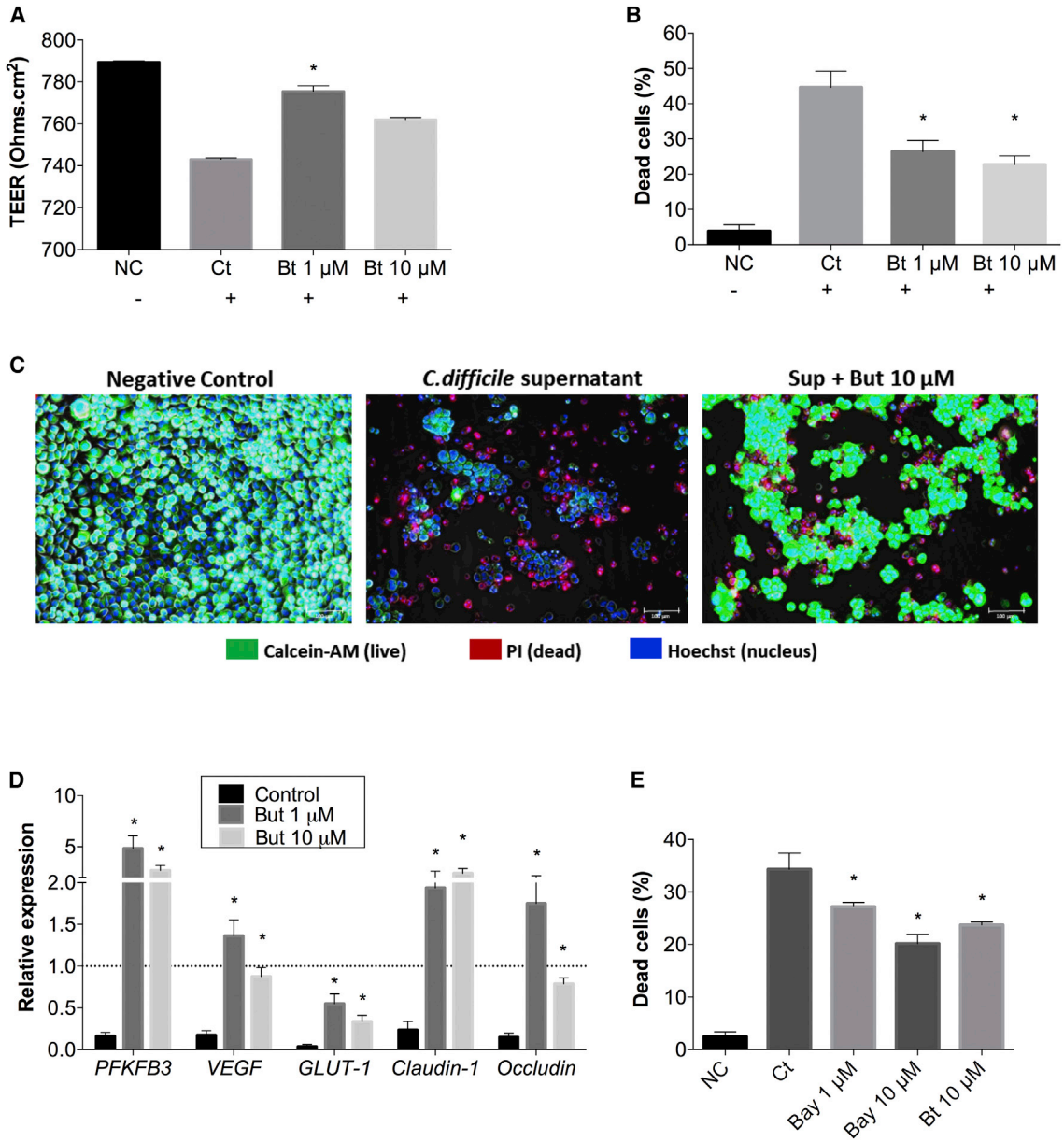

Figure 4. Butyrate Increases the Resistance of IECs to *C. difficile* Toxins

(A) Analysis of barrier integrity by TEER of HCT116 monolayer cells incubated for 48 h with *C. difficile* supernatant. NC, negative control (cells without toxins or treatment); Ct, cells incubated with *C. difficile* supernatant; Bt, cells incubated with *C. difficile* supernatant plus 1 or 10 μM butyrate (n = 6).

(B and C) Analysis of epithelial cell cytotoxicity 48 h after exposure to *C. difficile* supernatant and treatment with 10 μM butyrate (n = 6–8). Percentage of dead cells (B) and representative examples of cells incubated with *C. difficile* supernatant and butyrate (C) are shown. Scale bars, 100 μm.

(D) qPCR analysis of HIF-1 target gene expression in HCT116 cells treated with *C. difficile* supernatant and butyrate (n = 6–8).

(E) Percentage of dead epithelial cells after treatment with butyrate or Bay85-3934 (Bay) and incubation with *C. difficile* supernatant (n = 4–5).

*$p < 0.05$ compared to control. See also Figure S4.

DISCUSSION

The maintenance of the host-microbiota balance is key for homeostasis in animals. CDI is a good example of the relevance of the microbiota-host equilibrium as disruptions in microbiota composition lead to the impairment of mechanisms involved in the resistance to *C. difficile* colonization, growth, and production of toxins. These toxins can damage epithelial cells and activate inflammatory responses that together contribute to infection (Bäumler and Sperandio, 2016).

SCFAs are important molecules in host-microbiota communication as they are directly associated with the modulation of the host immune system and metabolism (Corrêa-Oliveira et al., 2016; Koh et al., 2016). A drastic reduction in intestinal SCFAs

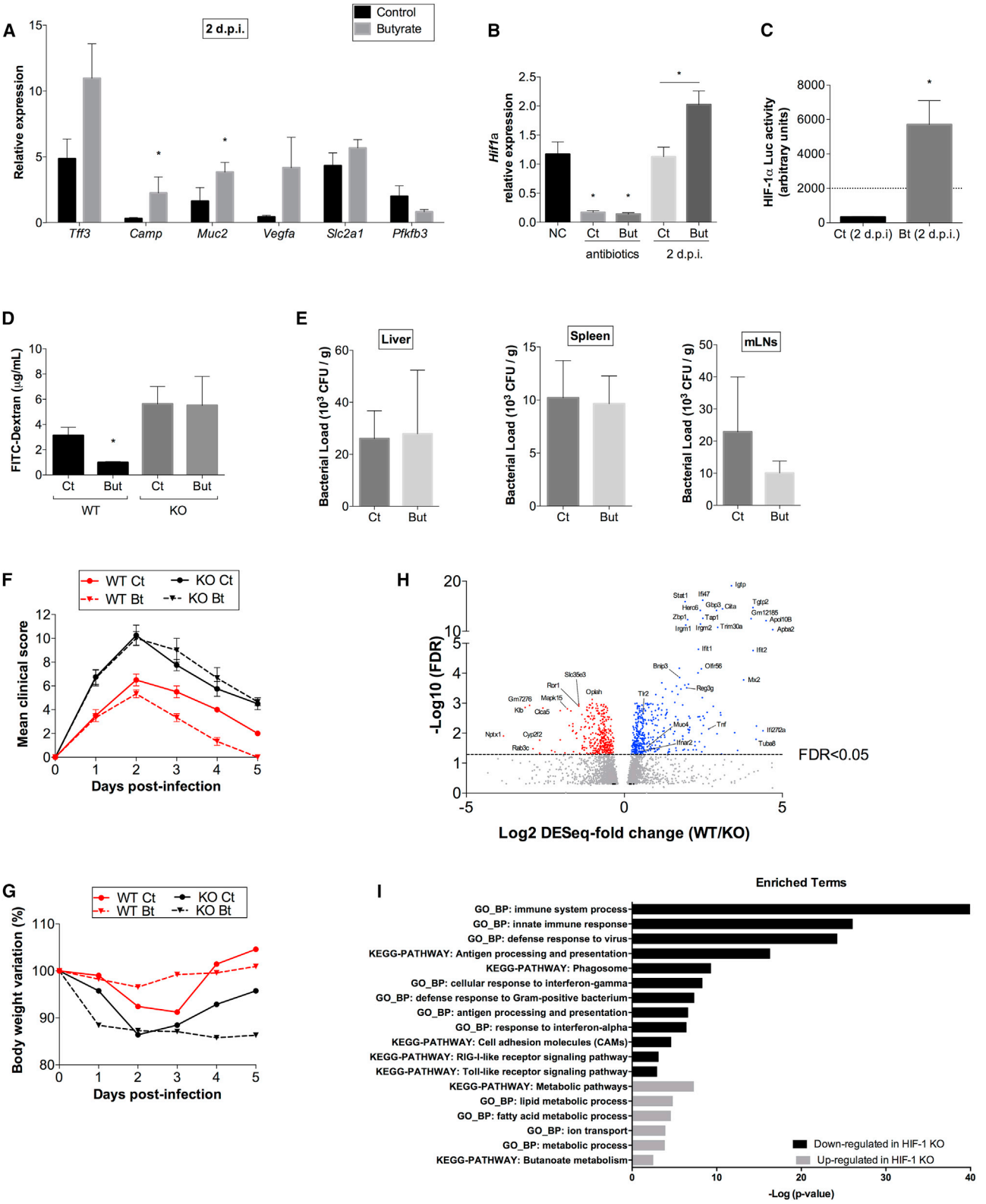

(legend on next page)

has been reported after antibiotic treatment and is associated with susceptibility to CDI (Antharam et al., 2013; Theriot et al., 2014). We observed that the restoration of intestinal concentrations of butyrate attenuated CDI in mice. This indicates that butyrate may be useful in preventing or attenuating CDI and relevant for the protective effect found with strategies such as the intake of dietary fiber (e.g., inulin, mixtures of microbiota-accessible carbohydrates) or SCFA-producing bacteria (e.g., *Bifidobacterium* spp.), associated with the reduction of *C. difficile* fitness in the intestinal tract (Hryckowian et al., 2018; Valdés-Varela et al., 2016).

Recent studies showed that SCFAs can diminish the severity and length of intestinal infections caused by different pathogenic bacteria such as *Salmonella enteric* serovar Typhimurium (Rivera-Chávez et al., 2016), *Shigella* (Raqib et al., 2006, 2012), and enterohemorrhagic *Escherichia coli* (EHEC) O157:H7 (Fukuda et al., 2012). Different molecular mechanisms and cell targets are involved, including direct/indirect effects on bacteria colonization and toxin production (Fukuda et al., 2012; Rivera-Chávez et al., 2016) and the stimulation of host-intestinal defenses (Raqib et al., 2006, 2012). Previous studies found that dietary fiber (the main source of SCFAs) or probiotic bacteria reduce CDI (Hryckowian et al., 2018; Valdés-Varela et al., 2016). Using butyrate supplementation, we found a protective effect against CDI, which was not dependent on the alterations in specific microbiota genera/phyla, *C. difficile* colonization, or toxin production, but on a direct effect on IECs.

A recent study found that butyrate restoration in mice led to improved IEC junction integrity and the mitigation of graft-versus-host disease (Mathewson et al., 2016). This effect of butyrate was independent of its impact on T cells, but it did involve the reduction of damage caused by allo-human leukocyte antigen (HLA)-reactive T cells in IECs (Mathewson et al., 2016), indicating that it increased their resistance to injury. As shown in other models, we found that butyrate had anti-inflammatory effects, including the inhibition of pro-inflammatory cytokines and attenuation of leukocyte recruitment to the inflammatory site (Smith et al., 2013; Vinolo et al., 2011). These effects may contribute to a balanced response that, while limiting tissue damage, is still effective in combating the infection (Buonomo and Petri, 2016). We also found that butyrate increased Treg and tolerogenic $CD103^+$ dendritic cells, as described by others (Arpaia et al., 2013; Singh et al., 2014; Smith et al., 2013; Tan et al., 2014). Although we cannot rule out the contribution of these effects on the mitigation of CDI by butyrate, our results indicate that its direct effects on IECs play a role in CDI protection, and HIF-1 is relevant in this context. We found that butyrate administration to mice in the CDI model increased *Hif1a* expression and stability. This explains the increased expression of HIF-1 target genes *in vivo*. Moreover, we found that the protective effect of butyrate in the CDI model was absent in *Hif1a*-deficient mice with no differences in intestinal permeability, translocation of bacteria, or clinical score, and no additive effect of butyrate was observed in mice with constitutive activation of this transcription factor ($Vhl^{\Delta IEC}$ mice). In contrast with the dependence of butyrate on HIF-1, acetate treatment exerted a protective effect that did not depend on the activation of this transcription factor (not shown).

Kelly et al. (2013) found that butyrate increases the stability of HIF-1 in IECs via the stimulation of metabolism and oxygen depletion. HIF-1 controls the expression of genes associated with inflammation, apoptosis, and intestinal barrier protection. Kelly et al. (2015) also found that butyrate treatment of Caco-2 cells reduced barrier permeability, a phenotype that was abrogated in HIF-1β knockdown cells. HIF-1 plays an important role in intestinal homeostasis and inflammatory conditions (Taylor and Colgan, 2017). In this context, Karhausen et al. (2004) observed the attenuation of the intestinal barrier during 2,4,6-trinitrobenzene sulfonic acid (TNBS) colitis in mice with the activation of HIF-1 and the opposite phenotype in $Hif1a^{\Delta IEC}$. Hirota et al. (2010) observed a reduction in intestinal injury and inflammation caused by *C. difficile* in mice that express *Hif1a* in IECs compared to *Hif1a*-deficient mice.

Our results expand these findings by demonstrating that butyrate increased the resistance of IECs to *C. difficile* toxins through an HIF-1α-dependent mechanism. We hypothesize that HIF-1 stabilization by butyrate may be protective during CDI, not only because it reduces intestinal epithelium damage but also because it improves the immune response against commensals, as indicated by the functional analysis of genes downregulated

Figure 5. Activation of HIF-1 in IECs Is Required for Butyrate Effects

(A) qPCR analysis of HIF-1 target genes in mice 2 days post-infection (n = 5). Results were normalized by values obtained with samples from non-infected mice and are presented as means ± SEMs.*$p < 0.05$ compared to infected control.

(B) qPCR analysis of *Hif1a* in the mouse colon after antibiotic treatment (day 0) and 2 days post-infection (n = 5).

(C) HIF-1 stability measured by luciferase activity in colon samples of ODD-luciferase reporter mice infected ± treatment with butyrate. Dashed line indicates the mean value obtained with samples from non-infected mice (n = 4). *$p < 0.05$ compared to control.

(D) Analysis of intestinal permeability by FITC-dextran quantification in the circulation of $Hif1a^{\Delta IEC}$ (KO) or control (WT) mice 2 days post-infection (n = 4). *$p < 0.05$ compared to control.

(E) qPCR analysis of the bacterial load translocated to the livers, mLNs, and spleens of HIF-1α epithelium-specific KO mice infected with *C. difficile* and treated with butyrate in the drinking water (n = 3–7).

(F and G) Analysis of (F) clinical score and (G) body weight variation of $Hif1a^{\Delta IEC}$ (KO)- or WT-infected mice ± butyrate in the drinking water (n = 5).

(H) Volcano plot of gene expression changes in IECs from butyrate-treated $Hif\text{-}1a^{\Delta IEC}$ and their control mice. Genes presented were obtained using DESeq2 (false discovery rate [FDR] <0.2). Genes over the dashed line have a significant difference (FDR) adjusted p value <0.05. The names of some selected genes with significant changes are shown.

(I) Bar chart presenting examples of Gene Ontology categories enriched based on the DEGs up- and downregulated in butyrate-treated $Hif1a^{\Delta IEC}$ mice. BP, biological process.

See also Figure S5.

in the absence of HIF-1 signaling, reducing their translocation to other tissues. These results indicate that interventions that restore butyrate intestinal levels may be an alternative form of therapy to patients with CDI.

STAR★METHODS

Detailed methods are provided in the online version of this paper and include the following:

- KEY RESOURCES TABLE
- CONTACT FOR REAGENT AND RESOURCE SHARING
- EXPERIMENTAL MODEL AND SUBJECT DETAILS
  - Mice
- CELL LINE CULTURE
- METHOD DETAILS
  - Model of infection
- SCFA TREATMENT
  - Determination of faecal bacterial load and 16S rRNA sequencing
  - Measurement of short-chain fatty acids
  - Histological analyses
  - Measurement of *in vitro* growth of C. difficile
  - Quantification of C. difficile TcdA/TcdB
  - Isolation of C. difficile from faeces
  - Measurement of cytokines in tissues
- QUANTITATIVE GENE EXPRESSION BY QPCR
  - Flow cytometry
  - Bacteria translocation
  - Measurement of intestinal permeability with FITC-Dextran
  - Measurement of luciferase activity in colon samples
  - Immunostaining for tight-junction proteins
  - Fluorescent *in situ* hybridization (FISH) preparation and analysis
  - Live/Dead assay
  - Transepithelial Electrical Resistance (TEER)
  - RNA-seq
- QUANTIFICATION AND STATISTICAL ANALYSIS
- DATA AND SOFTWARE AVAILABILITY

SUPPLEMENTAL INFORMATION

Supplemental Information can be found online at https://doi.org/10.1016/j.celrep.2019.03.054.

ACKNOWLEDGMENTS

This study was supported by Fundação de Amparo à Pesquisa do Estado de São Paulo (FAPESP; grants 2012/10653-9, 2013/06810-4, 2014/03002-7, 2015/06134-4, 2017/16280-3, and 2018/01753-6), Funcamp, National Council for Scientific and Technological Development (CNPq), Coordenação de Aperfeiçoamento de Pessoal de Nível Superior - Brasil (CAPES) - Finance Code 001, a Newton Advanced Fellowship by the Royal Society (between M.A.R.V. and P.V.-W.). J.L.F., L.P.P., B.K.S., R.O.C., Y.T.M., and T.C. are recipients of fellowships from FAPESP (2017/06577-9, 2018/02208-1, 2017/25679-7, 2016/23142-3, 2017/01451-7, and 2017/26366-2). A.M.T. was supported by a fellowship from FAPESP (2015/01507-7). We thank Juri Kazakevych for help with the RNA sequencing analyses and Maria Teresa Pedrosa Silva Clerici for the formulation of the diets.

AUTHOR CONTRIBUTIONS

Conceptualization, J.L.F. and M.A.R.V.; Methodology, J.L.F., J.S.F., D.M.F., P.J.B., E.L.S.S., T.C., S.E.G., and A.M.T.; Investigation, J.L.F., J.S.F., D.M.F., P.J.B., E.L.S.S., T.C., S.E.G., S.R.C., A.M.T., L.P.P., B.K.S., R.O.C., M.C.A., and Y.T.M.; Original Draft, J.L.F. and M.A.R.V.; Review & Editing, J.L.F., D.M.F., N.O.S.C., F.S.M., R.O.C., A.M.T., J.C.S., F.L.F., H.G.R., S.R.C., M.B.J., A.S.F., P.V.-W., and M.A.R.V.; Visualization, J.L.F., D.M.F., P.J.B., N.O.S.C., S.E.G., A.M.T., J.C.S., T.C., L.P.P., B.K.S., R.O.C., M.C.A., Y.T.M., F.L.F., H.G.R., S.R.C., M.B.J., A.S.F., P.V.-W., and M.A.R.V.; Funding Acquisition, P.V.-W. and M.A.R.V.; Resources, D.M.F., N.O.S.C., J.C.S., H.G.R., S.R.C., F.L.F., M.B.J., A.S.F., P.V.-W., and M.A.R.V.; Supervision, N.O.S.C., P.V.-W., and M.A.R.V.

DECLARATION OF INTERESTS

The authors declare no competing interests.

Received: September 4, 2018
Revised: January 17, 2019
Accepted: March 13, 2019
Published: April 16, 2019

REFERENCES

Antharam, V.C., Li, E.C., Ishmael, A., Sharma, A., Mai, V., Rand, K.H., and Wang, G.P. (2013). Intestinal dysbiosis and depletion of butyrogenic bacteria in Clostridium difficile infection and nosocomial diarrhea. J. Clin. Microbiol. *51*, 2884–2892.

Arpaia, N., Campbell, C., Fan, X., Dikiy, S., van der Veeken, J., deRoos, P., Liu, H., Cross, J.R., Pfeffer, K., Coffer, P.J., and Rudensky, A.Y. (2013). Metabolites produced by commensal bacteria promote peripheral regulatory T-cell generation. Nature *504*, 451–455.

Bäumler, A.J., and Sperandio, V. (2016). Interactions between the microbiota and pathogenic bacteria in the gut. Nature *535*, 85–93.

Buffie, C.G., Bucci, V., Stein, R.R., McKenney, P.T., Ling, L., Gobourne, A., No, D., Liu, H., Kinnebrew, M., Viale, A., et al. (2015). Precision microbiome reconstitution restores bile acid mediated resistance to Clostridium difficile. Nature *517*, 205–208.

Buonomo, E.L., and Petri, W.A. (2016). The microbiota and immune response during Clostridium difficile infection. Anaerobe *41*, 79–84.

Caporaso, J.G., Bittinger, K., Bushman, F.D., DeSantis, T.Z., Andersen, G.L., and Knight, R. (2010a). PyNAST: a flexible tool for aligning sequences to a template alignment. Bioinformatics *26*, 266–267.

Caporaso, J.G., Kuczynski, J., Stombaugh, J., Bittinger, K., Bushman, F.D., Costello, E.K., Fierer, N., Peña, A.G., Goodrich, J.K., Gordon, J.I., et al. (2010b). QIIME allows analysis of high-throughput community sequencing data. Nat. Methods *7*, 335–336.

Chen, X., Katchar, K., Goldsmith, J.D., Nanthakumar, N., Cheknis, A., Gerding, D.N., and Kelly, C.P. (2008). A mouse model of Clostridium difficile-associated disease. Gastroenterology *135*, 1984–1992.

Cohen, D., Fernandez, D., Lázaro-Diéguez, F., and Müsch, A. (2011). The serine/threonine kinase Par1b regulates epithelial lumen polarity via IRSp53-mediated cell-ECM signaling. J. Cell Biol. *192*, 525–540.

Corrêa-Oliveira, R., Fachi, J.L., Vieira, A., Sato, F.T., and Vinolo, M.A. (2016). Regulation of immune cell function by short-chain fatty acids. Clin. Transl. Immunology *5*, e73.

DeSantis, T.Z., Hugenholtz, P., Larsen, N., Rojas, M., Brodie, E.L., Keller, K., Huber, T., Dalevi, D., Hu, P., and Andersen, G.L. (2006). Greengenes, a chimera-checked 16S rRNA gene database and workbench compatible with ARB. Appl. Environ. Microbiol. *72*, 4.

Edgar, R.C. (2013). UPARSE: highly accurate OTU sequences from microbial amplicon reads. Nat. Methods *10*, 996–998.

Fellows, R., Denizot, J., Stellato, C., Cuomo, A., Jain, P., Stoyanova, E., Balázsi, S., Hajnády, Z., Liebert, A., Kazakevych, J., et al. (2018). Microbiota derived short chain fatty acids promote histone crotonylation in the colon through histone deacetylases. Nat. Commun. *9*, 105.

Fukuda, S., Toh, H., Taylor, T.D., Ohno, H., and Hattori, M. (2012). Acetate-producing bifidobacteria protect the host from enteropathogenic infection via carbohydrate transporters. Gut Microbes *3*, 449–454.

Galvão, I., Tavares, L.P., Corrêa, R.O., Fachi, J.L., Rocha, V.M., Rungue, M., Garcia, C.C., Cassali, G., Ferreira, C.M., Martins, F.S., et al. (2018). The Metabolic Sensor GPR43 Receptor Plays a Role in the Control of *Klebsiella pneumoniae* Infection in the Lung. Front. Immunol. *9*, 142.

Hall, J.A., Grainger, J.R., Spencer, S.P., and Belkaid, Y. (2011). The role of retinoic acid in tolerance and immunity. Immunity *35*, 13–22.

Hasegawa, M., Yada, S., Liu, M.Z., Kamada, N., Muñoz-Planillo, R., Do, N., Núñez, G., and Inohara, N. (2014). Interleukin-22 regulates the complement system to promote resistance against pathobionts after pathogen-induced intestinal damage. Immunity *41*, 620–632.

Hirota, S.A., Fines, K., Ng, J., Traboulsi, D., Lee, J., Ihara, E., Li, Y., Willmore, W.G., Chung, D., Scully, M.M., et al. (2010). Hypoxia-inducible factor signaling provides protection in Clostridium difficile-induced intestinal injury. Gastroenterology *139*, 259–69.e3.

Hryckowian, A.J., Van Treuren, W., Smits, S.A., Davis, N.M., Gardner, J.O., Bouley, D.M., and Sonnenburg, J.L. (2018). Microbiota-accessible carbohydrates suppress Clostridium difficile infection in a murine model. Nat. Microbiol. *3*, 662–669.

Johanesen, P.A., Mackin, K.E., Hutton, M.L., Awad, M.M., Larcombe, S., Amy, J.M., and Lyras, D. (2015). Disruption of the Gut Microbiome: Clostridium difficile Infection and the Threat of Antibiotic Resistance. Genes (Basel) *6*, 1347–1360.

Karhausen, J., Furuta, G.T., Tomaszewski, J.E., Johnson, R.S., Colgan, S.P., and Haase, V.H. (2004). Epithelial hypoxia-inducible factor-1 is protective in murine experimental colitis. J. Clin. Invest. *114*, 1098–1106.

Kelly, C.J., Glover, L.E., Campbell, E.L., Kominsky, D.J., Ehrentraut, S.F., Bowers, B.E., Bayless, A.J., Saeedi, B.J., and Colgan, S.P. (2013). Fundamental role for HIF-1α in constitutive expression of human β defensin-1. Mucosal Immunol. *6*, 1110–1118.

Kelly, C.J., Zheng, L., Campbell, E.L., Saeedi, B., Scholz, C.C., Bayless, A.J., Wilson, K.E., Glover, L.E., Kominsky, D.J., Magnuson, A., et al. (2015). Crosstalk between Microbiota-Derived Short-Chain Fatty Acids and Intestinal Epithelial HIF Augments Tissue Barrier Function. Cell Host Microbe *17*, 662–671.

Kim, M.H., Kang, S.G., Park, J.H., Yanagisawa, M., and Kim, C.H. (2013). Short-chain fatty acids activate GPR41 and GPR43 on intestinal epithelial cells to promote inflammatory responses in mice. Gastroenterology *145*, 396–406.e1–10.

Koh, A., De Vadder, F., Kovatcheva-Datchary, P., and Bäckhed, F. (2016). From Dietary Fiber to Host Physiology: Short-Chain Fatty Acids as Key Bacterial Metabolites. Cell *165*, 1332–1345.

Kuehne, S.A., Cartman, S.T., Heap, J.T., Kelly, M.L., Cockayne, A., and Minton, N.P. (2010). The role of toxin A and toxin B in *Clostridium difficile* infection. Nature *467*, 711–713.

Lamont, R.J., and Hajishengallis, G. (2015). Polymicrobial synergy and dysbiosis in inflammatory disease. Trends Mol. Med. *21*, 172–183.

Li, Y., Figler, R.A., Kolling, G., Bracken, T.C., Rieger, J., Stevenson, R.W., Linden, J., Guerrant, R.L., and Warren, C.A. (2012). Adenosine A2A receptor activation reduces recurrence and mortality from Clostridium difficile infection in mice following vancomycin treatment. BMC Infect. Dis. *12*, 342.

Lozupone, C., and Knight, R. (2005). UniFrac: a new phylogenetic method for comparing microbial communities. Appl. Environ. Microbiol. *71*, 8228–8235.

Martin, M. (2011). Cutadapt removes adapter sequences from high-throughput sequencing reads. EMBnet.J. *17*, 10–12.

Martin, J.S., Monaghan, T.M., and Wilcox, M.H. (2016). Clostridium difficile infection: epidemiology, diagnosis and understanding transmission. Nat. Rev. Gastroenterol. Hepatol. *13*, 206–216.

Maslowski, K.M., Vieira, A.T., Ng, A., Kranich, J., Sierro, F., Yu, D., Schilter, H.C., Rolph, M.S., Mackay, F., Artis, D., et al. (2009). Regulation of inflammatory responses by gut microbiota and chemoattractant receptor GPR43. Nature *461*, 1282–1286.

Mathewson, N.D., Jenq, R., Mathew, A.V., Koenigsknecht, M., Hanash, A., Toubai, T., Oravecz-Wilson, K., Wu, S.R., Sun, Y., Rossi, C., et al. (2016). Gut microbiome-derived metabolites modulate intestinal epithelial cell damage and mitigate graft-versus-host disease. Nat. Immunol. *17*, 505–515.

Molloy, M.J., Grainger, J.R., Bouladoux, N., Hand, T.W., Koo, L.Y., Naik, S., Quinones, M., Dzutsev, A.K., Gao, J.L., Trinchieri, G., et al. (2013). Intraluminal containment of commensal outgrowth in the gut during infection-induced dysbiosis. Cell Host Microbe *14*, 318–328.

Parks, D.H., Tyson, G.W., Hugenholtz, P., and Beiko, R.G. (2014). STAMP: statistical analysis of taxonomic and functional profiles. Bioinformatics *30*, 3123–3124.

Price, M.N., Dehal, P.S., and Arkin, A.P. (2009). FastTree: computing large minimum evolution trees with profiles instead of a distance matrix. Mol. Biol. Evol. *26*, 1641–1650.

Raqib, R., Sarker, P., Bergman, P., Ara, G., Lindh, M., Sack, D.A., Nasirul Islam, K.M., Gudmundsson, G.H., Andersson, J., and Agerberth, B. (2006). Improved outcome in shigellosis associated with butyrate induction of an endogenous peptide antibiotic. Proc. Natl. Acad. Sci. USA *103*, 9178–9183.

Raqib, R., Sarker, P., Mily, A., Alam, N.H., Arifuzzaman, A.S., Rekha, R.S., Andersson, J., Gudmundsson, G.H., Cravioto, A., and Agerberth, B. (2012). Efficacy of sodium butyrate adjunct therapy in shigellosis: a randomized, double-blind, placebo-controlled clinical trial. BMC Infect. Dis. *12*, 111.

Rea, M.C., Dobson, A., O'Sullivan, O., Crispie, F., Fouhy, F., Cotter, P.D., Shanahan, F., Kiely, B., Hill, C., and Ross, R.P. (2011). Effect of broad- and narrow-spectrum antimicrobials on Clostridium difficile and microbial diversity in a model of the distal colon. Proc. Natl. Acad. Sci. USA *108* (*Suppl 1*), 4639–4644.

Rivera-Chávez, F., Zhang, L.F., Faber, F., Lopez, C.A., Byndloss, M.X., Olsan, E.E., Xu, G., Velazquez, E.M., Lebrilla, C.B., Winter, S.E., and Bäumler, A.J. (2016). Depletion of butyrate-producing *Clostridia* from the gut microbiota drives an aerobic luminal expansion of *Salmonella*. Cell Host Microbe *19*, 443–454.

Rodriguez, C., Taminiau, B., Van Broeck, J., Delmée, M., and Daube, G. (2015). Clostridium difficile infection and intestinal microbiota interactions. Microb. Pathog. *89*, 201–209.

Schmieder, R., and Edwards, R. (2011). Quality control and preprocessing of metagenomic datasets. Bioinformatics *27*, 863–864.

Singh, N., Gurav, A., Sivaprakasam, S., Brady, E., Padia, R., Shi, H., Thangaraju, M., Prasad, P.D., Manicassamy, S., Munn, D.H., et al. (2014). Activation of Gpr109a, receptor for niacin and the commensal metabolite butyrate, suppresses colonic inflammation and carcinogenesis. Immunity *40*, 128–139.

Smith, P.M., Howitt, M.R., Panikov, N., Michaud, M., Gallini, C.A., Bohlooly-Y, M., Glickman, J.N., and Garrett, W.S. (2013). The microbial metabolites, short-chain fatty acids, regulate colonic Treg cell homeostasis. Science *341*, 569–573.

Stecher, B., and Hardt, W.D. (2008). The role of microbiota in infectious disease. Trends Microbiol. *16*, 107–114.

Tan, J., McKenzie, C., Potamitis, M., Thorburn, A.N., Mackay, C.R., and Macia, L. (2014). The role of short-chain fatty acids in health and disease. Adv. Immunol. *121*, 91–119.

Taylor, C.T., and Colgan, S.P. (2017). Regulation of immunity and inflammation by hypoxia in immunological niches. Nat. Rev. Immunol. *17*, 774–785.

Theriot, C.M., Koenigsknecht, M.J., Carlson, P.E., Jr., Hatton, G.E., Nelson, A.M., Li, B., Huffnagle, G.B., Z Li, J., and Young, V.B. (2014). Antibiotic-induced shifts in the mouse gut microbiome and metabolome increase susceptibility to Clostridium difficile infection. Nat. Commun. *5*, 3114.

Valdés-Varela, L., Hernández-Barranco, A.M., Ruas-Madiedo, P., and Gueimonde, M. (2016). Effect of Bifidobacterium upon Clostridium difficile Growth and Toxicity When Co-cultured in Different Prebiotic Substrates. Front. Microbiol. *7*, 738.

van Nood, E., Vrieze, A., Nieuwdorp, M., Fuentes, S., Zoetendal, E.G., de Vos, W.M., Visser, C.E., Kuijper, E.J., Bartelsman, J.F., Tijssen, J.G., et al. (2013). Duodenal infusion of donor feces for recurrent Clostridium difficile. N. Engl. J. Med. *368*, 407–415.

Vieira, A.T., Galvão, I., Macia, L.M., Sernaglia, E.M., Vinolo, M.A.R., Garcia, C.C., Tavares, L.P., Amaral, F.A., Sousa, L.P., Martins, F.S., et al. (2017). Dietary fiber and the short-chain fatty acid acetate promote resolution of neutrophilic inflammation in a model of gout in mice. J. Leukoc. Biol. *101*, 275–284.

Vinolo, M.A., Ferguson, G.J., Kulkarni, S., Damoulakis, G., Anderson, K., Bohlooly-Y, M., Stephens, L., Hawkins, P.T., and Curi, R. (2011). SCFAs induce mouse neutrophil chemotaxis through the GPR43 receptor. PLoS One *6*, e21205.

Wang, H.F., Feng, L., and Niu, D.K. (2007). Relationship between mRNA stability and intron presence. Biochem. Biophys. Res. Commun. *354*, 203–208.

STAR★METHODS

KEY RESOURCES TABLE

REAGENT or RESOURCE	SOURCE	IDENTIFIER
Antibodies		
Anti-mouse CD16/32, FITC, clone 2.4G2.	BD Biosciences	Cat# 553144, RRID: AB_394659
Anti-mouse CD11b, APC-Cy7, clone M1/70.	BioLegend	Cat# 101226; RRID: AB_830642
Anti-mouse CD11c, PE-Cy7, clone N418.	BioLegend	Cat# 117317; RRID: AB_493569
Anti-mouse CD45.2, APC-eFluor780, clone 104.	eBioscience	Cat# 47-0454-82; RRID: AB_1272175
Anti-mouse CD64, PE, clone X54-517.1.	BioLegend	Cat# 139304; RRID: AB_10612740
Anti-mouse CD103, APC, clone 2E7.	BioLegend	Cat# 121413; RRID: AB_1227503
Anti-mouse F4/80, PE-Cy7, clone BM8.	BioLegend	Cat# 123114; RRID: AB_893478
Anti-mouse MHCII (I-A/I-E), Pacific blue, clone M5/114.15.2.	BioLegend	Cat# 107620; RRID: AB_493527
Anti-mouse CD3, APC-Cy7, clone 145-2C11	BioLegend	Cat# 100330; RRID: AB_1877170
Anti-mouse CD8, APC, clone 3B5.	Thermo Fisher	Cat# MHCD0805; RRID: AB_10392701
Anti-mouse CD4, FITC, clone RM4-4.	BioLegend	Cat# 100510; RRID: AB_312713
Anti-mouse/rat Foxp3, eFluor660, clone FJK-16 s	eBioscience	Cat# 50-5773-82; RRID: AB_11218868
Anti-mouse Ly6C, Percp/Cy5.5, clone HK1.4.	BioLegend	Cat# 128012; RRID: AB_1659241
Anti-mouse Ly6G, PE, clone 1A8.	BioLegend	Cat# 127608; RRID: AB_1186099
Anti-mouse CD19, APC, clone 1D3.	BioLegend	Cat# 152410; RRID: AB_2629839
Anti-mouse CD161 (NK1.1), Alexa Fluor-488, clone PK136.	StemCell	Cat# 60103AD; RRID: AB_2783005
Anti-mouse Lyve-1, eFluor 660, clone ALY7.	Thermo Fisher	Cat# 50-0443-80; RRID: AB_10598060
Anti-mouse Siglec-F, PE, clone E50-2440.	BD Biosciences	Cat# 562757; RRID: AB_2687994
Anti-mouse TCR-beta, Percp/Cy5.5, clone H57-597.	BioLegend	Cat# 109228; RRID: AB_1575173
Anti-rabbit claudin-1 clone MH25	Thermo Fisher	Cat# 71-7800; RRID: AB_2533997
Anti-rabbit IgG polyclonal, Alexa Fluor 488.	Thermo Fisher	Cat# A-11034, RRID: AB_2576217
Bacterial and Virus Strains		
Clostridium difficile VPI 10463	Dr. Mário Júlio Ávila Campos	N/A
Escherichia coli	Dr. Marcelo Lancelotti	N/A
Chemicals, Peptides, and Recombinant Proteins		
kanamycin	Sigma-Aldrich	Cat# K1876-5G
gentamicin	Sigma-Aldrich	Cat# G1914-5G
colistin	Sigma-Aldrich	Cat# C4461-100MG
metronidazole	Sigma-Aldrich	Cat# M3761-5G
vancomycin	Sigma-Aldrich	Cat# V2002-1G
clindamycin	Sigma-Aldrich	Cat# C5269-50MG
acetic acid	Sigma-Aldrich	Cat# A6283-1L
butyric acid	Sigma-Aldrich	Cat# B103500-1L
Tributyrin	Sigma-Aldrich	Cat# W222399
Brain Heart Infusion (BHI) agar	Sigma-Aldrich	Cat# 70138-500G
Brain Heart Infusion Broth	Sigma-Aldrich	Cat# 53286-500G
Cycloserine-Cefoxitin-Fructose-Agar (CCFA)	AnaeroGRO	Cat# AG501
Clostridium difficile Supplement	Sigma-Aldrich	Cat# 17122-5VL
Yeast Extract	Sigma-Aldrich	Cat# 92144-500G-F
Hemin	Sigma-Aldrich	Cat# H9039-1G
Menadione	Sigma-Aldrich	Cat# M5625-25G
Formaldehyde solution	Sigma-Aldrich	Cat# 252549-1L
Glutaraldehyde solution	Sigma-Aldrich	Cat# G7651-10ML

(*Continued on next page*)

Continued

REAGENT or RESOURCE	SOURCE	IDENTIFIER
Histologic historesin	Leica	Cat# 7592
Giemsa Stain, Modified Solution	Sigma-Aldrich	Cat# 32884-250ML
Protease inhibitors	ThermoFisher	Cat# 78430
Power SYBR Green PCR Master Mix	Applied Biosystems	Cat# 4367659
RPMI-1640 medium	Vitrocell Embriolife	Cat# R0009
Deoxyribonuclease I from bovine pancreas	Sigma-Aldrich	Cat# DN25
Streptomycin sulfate	Sigma-Aldrich	Cat# S6501
Penicillin	Sigma-Aldrich	Cat# 1502701
HEPES	HyClone	Cat# SH30237.01
Fetal Bovine Serum	Corning	Cat# MT35016CV
β-mercaptoethanol	Sigma-Aldrich	Cat# M6250-10ML
0.5M EDTA pH8.0	Invitrogen	Cat# AM9261
DL-Dithiothreitol (DTT)	Sigma-Aldrich	Cat# D9779
Collagenase IV	Sigma-Aldrich	Cat# C5138-500MG
Ionomycin calcium salt	Sigma-Aldrich	Cat# I0634
L-glutamine	Sigma-Aldrich	Cat# G3126
Sodium Pyruvate	Sigma-Aldrich	Cat# P2256
MEM nonessential amino acids	ThermoFisher	Cat# 11140050
Tissue-Tek OCT Compound	O.C.T. Compound	Cat# 25608-930
Tris-HCl	Sigma-Aldrich	Cat# T5941-500G
NaCl	Sigma-Aldrich	Cat# S9888-500G
sodium dodecyl sulfate	Sigma-Aldrich	Cat# L3771-100G
DMEM medium	ThermoFisher	Cat# 11966-025
Dulbecco's (D)-PBS	Sigma-Aldrich	Cat# D4031-1L
Calcein-AM	Sigma-Aldrich	Cat# 17783-1MG
Propidium iodide	Sigma-Aldrich	Cat# P4170-10MG
Triton X-100	Merck Millipore	Cat# 1086431000
Hanks' Balanced Salt solution 10X	Sigma-Aldrich	Cat# H4641-500ML
Critical Commercial Assays		
PureLink™ Microbiome DNA Purification	ThermoFisher	Cat# A29790
Ridascreen® *C. difficile* Toxin A/B	R-Biopharm	Cat# C0801
Duo Set Kit: TNF-α	R & D System	Cat# DY008
Duo Set Kit: IL-6	R & D System	Cat# DY406
Duo Set Kit: IL-1β	R & D System	Cat# DY401
Duo Set Kit: IL-10	R & D System	Cat# DY417
Duo Set Kit: MIP-2 (Cxcl-2)	R & D System	Cat# DY452
Duo Set Kit: KC (Cxcl-1)	R & D System	Cat# DY453
PureLink™ RNA Mini Kit	ThermoFisher	Cat# 12183020
High-Capacity cDNA Reverse Transcription	Applied Biosystems	Cat# 4368814
Dual Luciferase Reporter Assay System	Promega Corporation	Cat# E1910
Deposited Data		
16S rDNA amplicon sequencing	This study	BioProject ID PRJNA486872
IECs RNA sequencing	This study	BioProject ID PRJNA515618
Experimental Models: Cell Lines		
HCT-116	Dr. Patrick Varga-Weisz	N/A
Experimental Models: Organisms/Strains		
C57BL/6J male mice	CEMIB - UNICAMP	N/A
Rag-1 deficient mice	USP, Ribeirão Preto-SP, Brazil	N/A

(*Continued on next page*)

Continued		
REAGENT or RESOURCE	SOURCE	IDENTIFIER
IL-10 deficient mice	Jackson Laboratories	JAX# 003968
Hif-1a floxed mice	Jackson Laboratories	JAX# 007561
Vhl floxed mice	Jackson Laboratories	JAX# 012933
Villin-Cre mice	Jackson Laboratories	JAX# 004586
ODD-luciferase mice	Jackson Laboratories	JAX# 006206
Foxp3-GFP mice	Jackson Laboratories	JAX# 023800
Germ-free Swiss mice	UFMG Belo Horizonte-MG, Brazil	N/A
Oligonucleotides		
Primers for quantitative PCR, see Table S2	This paper	N/A
Bacteria probes, FITC-conjugated.	Sigma-Aldrich	N/A
Ulex europaeus agglutinin-I, TRITC-conjugated, L4889.	Sigma-Aldrich	Cat# L4889
Software and Algorithms		
GraphPad Prim 5.0	GraphPad Software	N/A
FlowJo LLC version 10.1.	Becton Dickinson	N/A
FACSDiva	BD Biosciences	N/A
ImageJ	National Institutes of Health	N/A
Gen5 software	Biotek	N/A
Applied Biosystems 7500 Real-Time PCR System	ThermoFisher	N/A
Other		
123count eBeads	ThermoFisher	Cat# 01-1234
AnaeroGen Oxoid	ThermoFisher	Cat# AN0025A
70- and 40-μm cell strainers	BD Biosciences	Cat# CLS431751-50EA
LIVE/DEAD fixable dead stain	Thermo Fisher	Cat# L34962
Fluorescein isothiocyanate–dextran	Sigma-Aldrich	Cat# 46944-100MG-F
DAPI	Sigma-Aldrich	Cat# D9542
Vectashield medium	Vector Laboratories	Cat# H-1200
Hoechst 33258 solution	ThermoFisher	Cat# 62249
SlowFade® Gold medium	ThermoFisher	Cat# S36936

CONTACT FOR REAGENT AND RESOURCE SHARING

Further information and requests for resources and reagents should be directed to and will be fulfilled by the Lead Contact, Marco Vinolo (mvinolo@unicamp.br).

EXPERIMENTAL MODEL AND SUBJECT DETAILS

Mice

The Multidisciplinary Centre for Biological Investigation (CEMIB - UNICAMP) provided adult C57BL/6J male mice. *Rag-1* deficient mice (*Rag1*$^{-/-}$) were from the CEDEME (UNIFESP). *Hif1a*$^{FL/FL}$, *Vhl*$^{FL/FL}$, Villin-Cre, ODD-luciferase and Foxp3-GFP mice were purchased from Jackson Laboratories or provided by collaborators and maintained in the Animal facility of the Department of Genetics, Evolution, Microbiology and Immunology. These strains were maintained in a C57BL/6J background. ODD-luciferase mice had an FVB background. Experiments with germ-free animals (Swiss mice) were performed in the Department of Microbiology, Institute of Biological Science of the Federal University of Minas Gerais. All mice used in this study were 6-12 wks-old. Only male mice were used. All mice were kept in regular filter-top cages with free access to sterile water and food. All animal procedures were approved by the Ethics Committee on Animal Use of the Institute of Biology (protocol numbers 3230-1/3742-1).

CELL LINE CULTURE

Human colon carcinoma cells (HCT116) were cultivated in DMEM medium supplemented with 10% fetal bovine serum, 2 mM L-glutamine and penicillin/streptomycin at 37°C with 5% CO_2. Cells were used until passage 20.

METHOD DETAILS

Model of infection

The *C. difficile* VPI 10463 strain was cultivated in BHI blood agar supplemented with hemin (5 μg/mL) and menadione (1 μg/mL) at 37°C in anaerobic atmosphere (AnaeroGen, Oxoid; ThermoFisher Scientific; Waltham, MA, USA) in jars. Mouse infections were performed as described (Chen et al., 2008). Briefly, mice were pre-treated with antibiotic mixture (0.4 mg/mL kanamycin, 0.035 mg/mL gentamicin, 0.035 mg/mL colistin, 0.215 mg/mL metronidazole and 0.045 mg/mL vancomycin; Sigma) added to drinking water for 4 days. Next, mice received one dose of clindamycin (10 mg/kg, i.p.) (Sigma). After 1 day, mice were infected with 1×10^8 colony forming units (CFUs) of *C. difficile* by gavage. Mice were weighed and monitored daily during the entire protocol with a clinical severity score that varied from 0 (normal) to 15, as described (Li et al., 2012) (Table S1).

SCFA TREATMENT

Animals received oral pre-treatment with 150 mM butyrate or placebo, as reported in other studies (Smith et al., 2013; Vieira et al., 2017). Butyrate treatment started one day before addition of antibiotics and continued throughout the protocol. In parallel, mice were treated with 3 g/kg tributyrin by gavage on days −1, 0 and 1 of colitis induction. In dietary experiments, mice received food containing different amounts of soluble fibers: a control diet, based on American Institute of Nutrition (AIN93) recommendations containing 5% cellulose; and one with high fiber supplemented with 5% cellulose and 25% inulin. Mice were pre-fed the different diets for 7 days.

Determination of faecal bacterial load and 16S rRNA sequencing

Faecal samples (50 mg) were used for extraction of microbial genomic DNA using the PureLink™ Microbiome DNA Purification kit (ThermoFisher Scientific). For bacterial load measurement, DNA was quantified by quantitative polymerase chain reaction (qPCR) using primers complementary to Eubacteria 16S rDNA (Table S2). A standard curve was constructed with serial dilutions of *E. coli* genomic DNA. Results were normalized to controls. Amplification and sequencing of 16 s rRNA was performed using Illumina MiSeq (Institute of Chemistry, University of São Paulo). Sequences of primers used for amplification of 16S rRNA V3-V4 variable regions are given in Table S2. Raw reads were filtered using Prinseqlite v.0.20.4 (Schmieder and Edwards, 2011) by removing sequences with average quality scores below 20. Resulting paired-end reads were overlapped using the merge program PEAR (v.0.9.10). Primers and adapters were trimmed using cutadapt v.1.12 (Martin, 2011) allowing maximum frequencies of 0.12 and 0.10 mismatches and indels for forward and reverse primers, respectively. Sequences shorter than 300 bp or those which were untrimmed were discarded. Pre-processed sequences were clustered into Operational Taxonomic Units (OTUs) using UPARSE (Edgar, 2013) with 97% similarity threshold. Taxonomy was assigned using the RDP classifier (v.2.2) (Wang et al., 2007). To investigate alpha and beta diversity, OTU tables were rarefied according to number of sequences of the smallest sample (22,584) and sequences were aligned to the greengene score set (DeSantis et al., 2006) using PyNAST (Caporaso et al., 2010a) with Qiime default parameters (QIIME v.1.9.1) (Caporaso et al., 2010b). A phylogenetic tree was built to calculate pairwise UniFrac (Lozupone and Knight, 2005) distances using FastTree (Price et al., 2009). Statistical analyses of beta diversity used the vegan R package function Adonis and its default value of 999 permutations (https://cran.r-project.org/web/packages/vegan/index.html). Differential abundance was calculated for differences between mean proportions of each treatment. Significance was determined using Welch's t test and Benjamini-Hochberg FDR correction available in STAMP (Parks et al., 2014). The data is deposited at NCBI's BioProject (ID: PRJNA486872).

Measurement of short-chain fatty acids

Fecal samples or colonic luminal content samples were harvested from mice as described (Fellows et al., 2018) for measurement of SCFAs. Chromatographic analyses were performed using a GCMS-QP2010 Ultra mass spectrometer (Shimadzu; ThermoFisher Scientific) and a 30 m × 0.25 mm fused-silica capillary Stabilwax column (Restek Corporation, Bellefonte, PA, USA) coated with 0.25-μm polyethylene glycol. Samples (1 μL) were injected at 250°C using a 25:1 split ratio. High-grade pure helium was used as carrier gas at 1.0 mL/min constant flow. Mass conditions were as follows: ionization voltage, 70 eV; ion source temperature, 200°C; full scan mode, 35–500 m/z with 0.2 s scan velocity. The runtime was 11.95 min.

Histological analyses

Mouse colons were harvested, opened longitudinally and fixed in 4% formalin/0.1% glutaraldehyde. Tissues were processed into historesin and 5-μm sections prepared for staining with Hematoxylin and eosin. Slides were analyzed using an Olympus Microscope (Mod. U-LH100HG). Samples were analyzed blindly using histological scores for each parameter (Table S3). Overall scores were the sums of each component and varied from 0 to 30.

Measurement of *in vitro* growth of C. difficile

Bacteria were incubated in 5 mL Brain Heart Infusion (BHI) agar containing 1-50 mM butyrate for 72 h in anaerobic atmosphere at 37°C. Optical density of the medium was read at 600 nm and the bacterial suspension diluted and plated in BHI agar to check for possible contaminations. The culture supernatant was used for measurement of toxins.

Quantification of C. difficile TcdA/TcdB

Toxins were measured in faecal samples and bacterial culture supernatants using the Ridascreen® *C. difficile* Toxin A/B ELISA kit (R-Biopharm; Darmstadt, Germany). Faecal samples were harvested on day 2 post infection, weighed and vortexed in 1 mL dilution buffer. Samples were left 10 min prior to decanting and the supernatant collected for measurement.

Isolation of C. difficile from faeces

Faecal samples harvested on day 2 post-infection were weighed, vortexed in 1 mL sterile PBS and left 10 min prior to decantation. Supernatants were diluted at 10^{-6} and 10^{-7} and plated on cycloserine-cefoxitin-fructose-agar supplemented with horse blood. Plates were incubated in an anaerobic atmosphere at 37°C for 4-5 days.

Measurement of cytokines in tissues

Colon samples (100 mg) were homogenized in PBS containing protease inhibitors (ThermoFisher Scientific). Samples were centrifuged 10 min at 2000 x g and supernatants used for measurement of TNF-α, IL-6, IL-1β, IL-10, Cxcl1 and Cxcl2 using the Duo Set ELISA kit (R&D System; Minneapolis, MN, USA).

QUANTITATIVE GENE EXPRESSION BY qPCR

Total RNA was extracted from colon, cecum and mesenteric lymph nodes using the PureLink™ RNA kit (Ambion). RNA was converted to cDNA using the High-Capacity cDNA Reverse Transcription Kit (Applied Biosystems; Foster City, CA, USA) and qPCR was performed using Power SYBR Green PCR Master Mix (Applied Biosystems) and primers indicated in Table S2. Quantification of gene expression was performed using a ΔΔ Ct method with β2-microglobulin as a reference gene.

Flow cytometry

Cells were isolated from colon, mesenteric lymph nodes (mLNs) and spleen as described by Hall et al. (2011). After removal of faecal contents, colon was incubated 20 min in RPMI-1640 medium containing 3% fetal bovine serum (FBS), 100 U/mL penicillin - 100 μg/mL streptomycin (Pen/Strep), 25mM HEPES, 50 mM β-mercaptoethanol (β-ME), 5 mM EDTA and 0.145 mg/mL of dithiothreitol (DTT) (Sigma). The epithelial layer was removed by agitation in serum-free RPMI containing 2 mM EDTA. Tissues were minced and digested with serum free RPMI containing: 25 mM HEPES, 50 μM β-ME, 1 mg/mL collagenase IV (Sigma) and 0.5 mg/mL DNase I (Sigma) by continuous stirring at 37°C for 25 min. Digests were diluted in RPMI containing 3% FBS, Pen/Strep, 25 mM HEPES and 50 mM β-ME, and mashed through 70- and 40-μm cell strainers (BD Biosciences; San Jose, CA, USA). Cells were centrifuged briefly and suspended in complete RPMI containing 10% FBS, Pen/Strep, 25 mM HEPES, 2 mM L-glutamine, 1 mM sodium pyruvate and 50 mM β-ME. For cell isolation from mLNs and spleen, tissues were minced with scissors and incubated 20 min at 37°C in 0.25 mg/mL collagenase IV/0.25 mg/mL DNase I followed by tissue mashing through 70 μm cell strainers. Cells were washed and suspended in complete RPMI. Dead cells were discriminated in all experiments using LIVE/DEAD fixable dead stain (ThermoFisher Scientific) and all staining steps carried out in media containing anti-CD16/32 (2.4G2 antibody). The following antibody clones were used: CD11b (M1/70), CD11c (N418), CD45.2 (104), CD64 (X54-517.1), CD103 (2E7), F4/80 (BM8), MHCII (I-A/I-E) (M5/114.15.2), Ly6C (HK1.4), Ly6G (1A8), CD19 (1D3), CD161 (NK1.1) (PK136), Lyve-1 (ALY7), Siglec F (E50-2440) and TCR-beta (H57-597). Cell acquisitions were performed on a BD LSR X20 cell analyzer (BD Biosciences) using FACSDiva software (BD Biosciences) and data analyzed using FlowJo software (TreeStar Inc.; Ashland, OR, USA).

Bacteria translocation

Spleen and liver were harvested on day 2 post-infection. Tissues were weighted and homogenized in 1 mL PBS using a tissue homogenizer under sterile conditions for 60 s. Homogenates were centrifuged 10 min at 2000 x g (4°C) and 100 μL supernatant plated on BHI agar plates supplemented with hemin and menadione. Plates were incubated in anaerobic jars or under aerobic conditions at 37°C. Colony counting was performed after 4-5 days. 16S rDNA gene levels were determined by qPCR.

Measurement of intestinal permeability with FITC-Dextran

Mice received 200 μL FITC-Dextran (70,000 Da; Sigma) suspension (250 mg/Kg) by gavage on day 2 of infection. After 4 h, mice were anesthetized, blood collected by caudal puncture and fluorescence readings performed in a Multi-Mode Microplate Reader (Synergy HT; Vermont, USA) at 485/528 nm (excitation/emission). A standard curve was prepared with serial dilutions of FITC-Dextran in PBS.

Measurement of luciferase activity in colon samples

Colon samples from ODD-luciferase mice were harvested and homogenized in lysis buffer. Luciferase activity was measured using Dual Luciferase Reporter Assay System (Promega Corporation; Madison, WI, USA). Protein concentrations were used for data normalization.

Immunostaining for tight-junction proteins

Colon fragments were harvested, washed with PBS and fixed 2 h in 4% formaldehyde. Tissues were embedded in Tissue-Tek OCT Compound (Sakura® Finetek, Torrance, CA, USA), snap frozen and stored at −80°C. Sections were cut (4 μm) using a cryostat and labeled overnight at 4°C with antibodies (1:50; anti-claudin-1 or 1:100; anti-occludin; ThermoFisher Scientific) after blocking non-specific binding sites with 1% BSA. A secondary antibody conjugated with AlexaFluor-488 (1:100; Sigma) was used for detection. DAPI (1:1000; Invitrogen; Carlsbad, CA, USA) was added and sections mounted in Vectashield medium (Vector Laboratories, Inc.; Burlingame, CA, USA). Markings were detected and photographed by confocal laser microscopy (CLSM; Bio-Rad MRC 1024;Bio-Rad, Richmond, CA, USA) through a 10x objective. To allow comparison between groups, green fluorescence intensity (485 ± 10/530 ± 12.5 nm excitation/emission) was measured using ImageJ software (National Institutes of Health, Bethesda, MD, USA) and expressed in arbitrary units.

Fluorescent *in situ* hybridization (FISH) preparation and analysis

FISH was performed as described by Molloy et al. (2013). Colon fragments were fixed in methacarn 3 h at 4°C and coronal slices (5-μm) obtained. After deparaniffization and rehydratation, sections were incubated in hybridization buffer [20 mM Tris-HCl, 0.9 M NaCl and 0.1% SDS (pH 7.2)] 10 min at 50°C. Next, sections were incubated with 100 nM bacteria probes (5′- > 3′: GCTGCCTCCCGTAGGAGT; FITC-conjugated; Sigma) in hybridization buffer in the dark, 4 h at 50°C, washed with 20 mM Tris-HCl, 0.9 M NaCl (pH 7.2) and incubated 2 h at room temperature in 20 μg/mL Lectin–*Ulexeuropaeus* agglutinin-I (UEA-I; TRITC-conjugated, Sigma). Sections were washed again, incubated 10 min with 10 μg/mL Hoechst 33258 solution and mounted with SlowFade® Gold medium (ThermoFisher Scientific). Images were acquired using a Zeiss LSM-780 confocal microscope (Carl Zeiss; Oberkochen, Germany). Samples were imaged with 63x/1.4NA oil-immersion objective at 3x with a 1024 × 1024 frame size. Qualitative analysis was performed and included the following features: presence/absence of mucus, bacterial load, bacterial translocation and epithelial morphology. Three apical extrusion zones of colon were randomly chosen to measure epithelium-luminal bacteria distance. The mean was used to calculate the distance between apical extrusion zones and the first bacterial focus in the gut.

Live/Dead assay

Cells were cultivated in 1:500 bacterial supernatant and 1, 10 or 100 μM butyrate in 96-well plates (1.0×10^5 cells/well). After 48 h, cells were washed gently using Dulbecco's (D)-PBS and media replaced by 100 μL Calcein-AM and propidium iodide (2 μM) in D-PBS and incubated 30 min at 37°C under 5% CO_2. Images were obtained using the Cytation 5 Cell Imaging Multi-Mode Reader and green fluorescence (485/530 nm, excitation/emission) of viable cells and red fluorescence (530/645 nm) of dead cells quantified using Gen5 software (Biotek, Winooski, VT, CA). The positive control was pre-incubation of cells with 0.1% Triton-X 15 min. To obtain *C. difficile* supernatants, the toxigenic strain VPI 10463 was cultured 24 h at 37°C in anaerobic conditions in BHI medium supplemented with hemin and menadione. The culture was centrifuged at 10,000 x g 5 min and supernatant used for treatment of HCT116 culture (1:500 ratio).

Transepithelial Electrical Resistance (TEER)

HCT116 cells (2.0×10^5 cells/mL) were cultured 24 h at 37°C in DMEM containing 10% FBS, 2 mM L-glutamine, and Pen/Strep in transwell permeable polyester supports (Corning Life Sciences; Tewksbury, MA, USA) (0.4 μm/pore, Costar) to approximate confluence. Cells were incubated with 1:500 *C. difficile* supernatant and different concentrations of butyrate 48 h at 37°C under 5% CO_2. Electrical resistance was measured by potential difference using electrodes and the EVOM2 and Endohm 24-SNAP system (World Precision Instruments, Sarasota, FL). Values were expressed as Ω/cm^2 resistance.

RNA-seq

IECs were isolated from the colon of infected (2 d.p.i.) mice treated with butyrate. Briefly, colons were opened longitudinally and washed three times with ice cold DPBS. IECs were isolated using 2 mM EDTA/HBSS at 37°C with shaking for 60 min. The tubes with colons were shaken in vortex for 20 s after every 10 min. The material was then filtered through a 100 μm followed by a 70 μm cell strainer. The extracted cells were pelleted at 475 × g at 4 °C for 10 min, washed in ice cold DPBS and counted in Neubauer chamber. Total RNA was extracted from 2×10^6 IECs using PureLink™ RNA Mini Kit (ThermoFisher). RNA quantification and integrity were measured on a BioAnalyzer RNA 6000 Pico chip (Agilent) and sent to BGI (Shenzhen, China) for cDNA library construction and sequencing. Sequencing was done using the BGISEQ-500 platform (read length 100 pb, paired-end) and, at least 20 million clean reads were obtained from each sample. The software SOAPnuke was used for removing adaptors reads, reads in which unknown bases are more than 5% and low quality reads. Reads were mapped to the mouse (GRCm38) reference genome and analyzed using SeqMonk software (version 0.34.1, Babraham Institute Bioinformatics - Cambridge, UK). Gene ontology analysis was done online in DAVID 6.8 (Database for Annotation, Visualization and Integrated Discovery).

QUANTIFICATION AND STATISTICAL ANALYSIS

Analyses were performed using GraphPad software 5.0 (San Diego, CA, USA). Differences were considered significant for $p < 0.05$. Results were first analyzed using D'Agostino/Shapiro-Wilk normality tests and compared by Student's t test or Mann Whitney test, as

appropriate. For more than two groups, differences were compared by one-way ANOVA followed by Tukey's post hoc test or Kruskal-Wallis followed by Dunn's test.

DATA AND SOFTWARE AVAILABILITY

The RNA-seq and 16S rDNA amplicon sequencing data reported in this paper have been deposited at BioProject NCBI, under accession numbers PRJNA515618 and PRJNA486872.

Cell Reports, Volume *27*

Supplemental Information

Butyrate Protects Mice from *Clostridium difficile*-Induced Colitis through an HIF-1-Dependent Mechanism

José Luís Fachi, Jaqueline de Souza Felipe, Laís Passariello Pral, Bruna Karadi da Silva, Renan Oliveira Corrêa, Mirella Cristiny Pereira de Andrade, Denise Morais da Fonseca, Paulo José Basso, Niels Olsen Saraiva Câmara, Éricka Lorenna de Sales e Souza, Flaviano dos Santos Martins, Suzana Eiko Sato Guima, Andrew Maltez Thomas, João Carlos Setubal, Yuli Thamires Magalhães, Fábio Luis Forti, Thamiris Candreva, Hosana Gomes Rodrigues, Marcelo Bispo de Jesus, Sílvio Roberto Consonni, Alessandro dos Santos Farias, Patrick Varga-Weisz, and Marco Aurélio Ramirez Vinolo

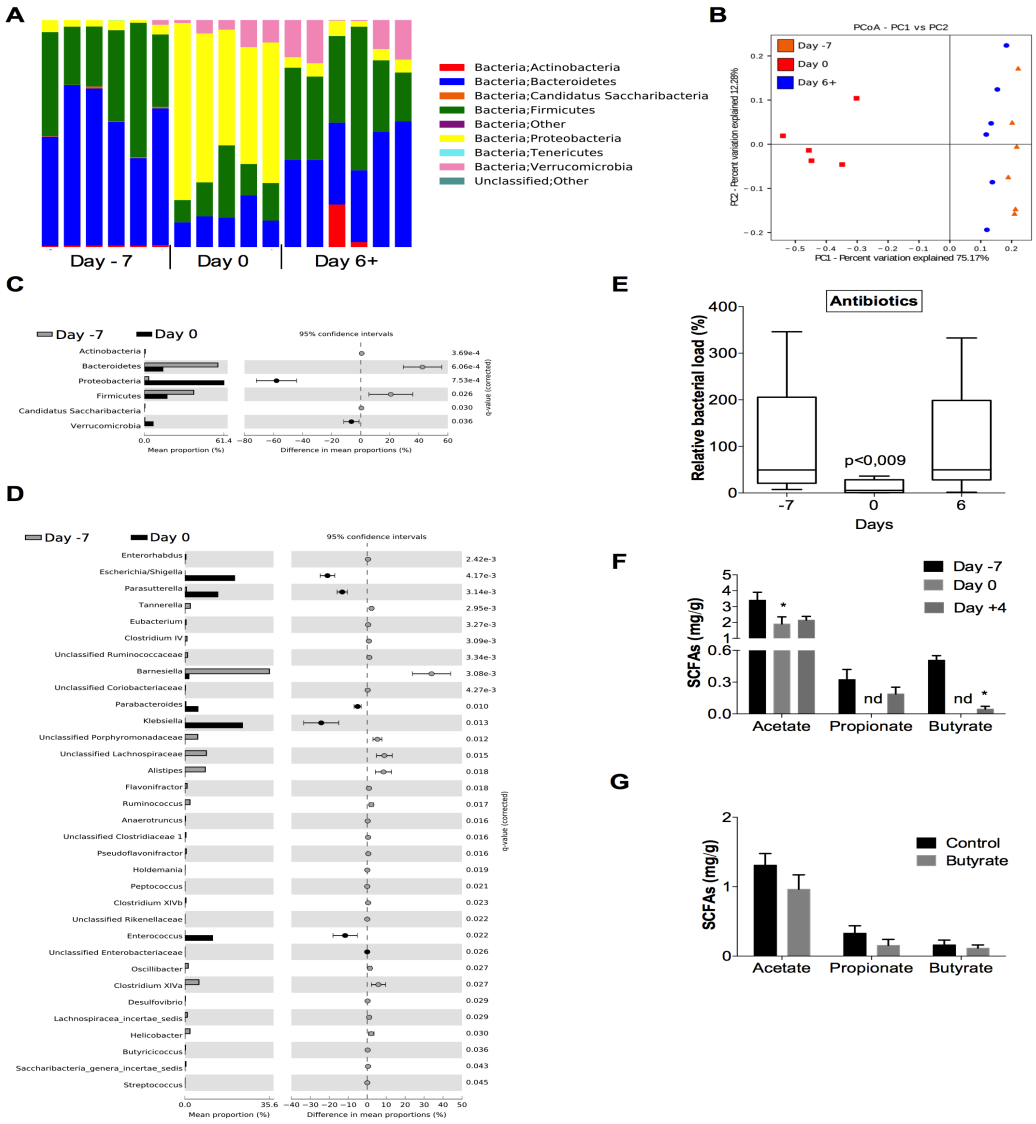

Figure S1. Microbiota changes after antibiotic treatment affect the SCFA-production, Related to Figure 1.

(A–D) Adult C57BL/6 mice (n = 5-6) were treated with a mixture of antibiotics added to the drinking water for 4 days and then received a single i.p. dose of clindamycin. One day later, these mice were susceptible to CDI (day 0). Samples were collected before treatment with antibiotic mix (day –7), after antibiotic treatment (day 0) and 6 days later, when mice were again resistant to infection (day 6+). (A) Fecal microbiota composition at the different time points. (B) PCoA plot using Bray-Curtis dissimilarity based on phylum-level OTUs from fecal microbiota of mice at different time points. (C) Significant differences at the phylum level between fecal microbiota of mice before and after antibiotic treatment. (D) Significant differences at bacterial genus level between fecal microbiota of mice before and after antibiotic treatment. (E) Relative bacterial load of feces by quantification of 16S DNA (n= 5-6). The bar indicates median ± min to max. (F) Measurement of SCFAs concentrations in fecal samples of mice at different time points. Results are presented as mean ± SEM (n= 3-4). Nd: not detected. * $p<0.05$, compared to day -7 condition. (G) Measurement of SCFAs concentrations in colon content of mice treated or not with butyrate. Results are presented as mean ± SEM (n= 4).

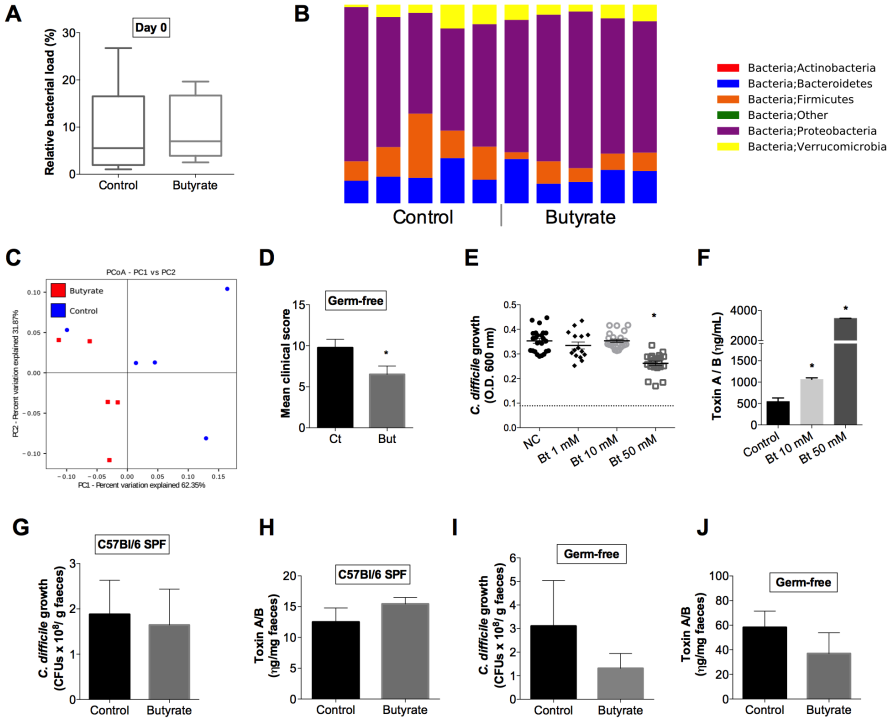

Figure S2. Protective effect of butyrate on CDI does not depend of its effect on intestinal microbiota or *C. difficile* colonization/toxin production, Related to Figure 2.
(A-B) Analysis of the effect of butyrate on the intestinal microbiota. Relative bacterial load and microbiota composition in the feces after antibiotic treatment (day 0) (A-C). The bar indicates median ± min to max (A) (n= 5-6). (B) Fecal microbiota composition of mice treated or not with butyrate. (C) PCoA plot using Bray-Curtis dissimilarity based on phylum-level OTUs from fecal microbiota of mice treated or not with butyrate. (D) Clinical score of butyrate and control germ-free mice on the second day of infection with 10^8 CFU of *C. difficile* (n = 6). Results are presented as mean ± SEM. * $p<0.05$, compared to the control. (E) *In vitro* growth of *C. difficile* in the presence of different concentrations of butyrate (n = 5 independent experiments with 5 replicates). The dashed line represents culture medium without bacterium. (F) Quantification of toxins A and B in culture supernatant by immunoassay (n = 5). (G and I) Isolation of *C. difficile* from faeces of adult male SPF (G) and germ-free (I) mice by stool plating in cycloserine, cefotoxin-fructose agar (CCFA) (n = 5-6). (H and J) Concentration of toxins A and B presents in the faeces of SPF (H) and germ-free (J) mice 2 days post-infection (n = 5-6). Results are presented as mean ± SEM. * $p<0.05$, compared to the control.

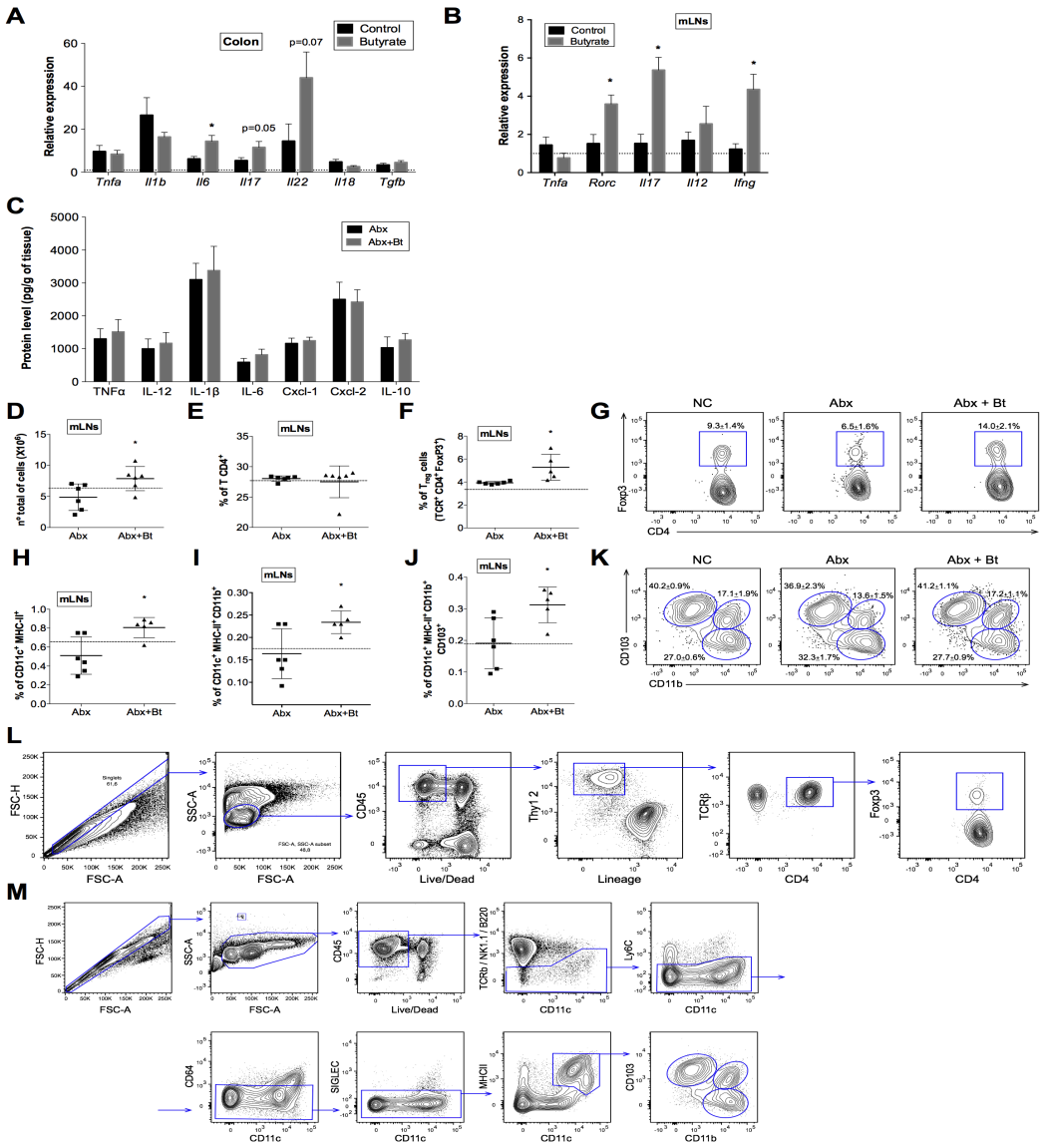

Figure S3. **Immunomodulatory effects of butyrate on CDI, Related to Figure 2**.
(A-B) The expression of inflammatory genes was measured by qPCR in the colon (A) and mesenteric lymph nodes (B) of mice 2 days post-infection (n = 8-10). Results were normalized by values obtained with samples from non-infected mice and are presented as mean ± SEM. * $p<0.05$, compared to the infected control without butyrate treatment. The dashed line represents the mean value of expression of the genes in non-infected mice. (C) Quantification of cytokines in colon of antibiotic (Abx) treated mice +/- butyrate (Bt) treatment. Results were normalized by tissue weight and presented as mean ± SEM (n=3-6). (D-J) Analysis of leukocyte populations in the mesenteric lymph nodes (mLNs) of mice after antibiotic therapy (Abx) +/- butyrate (Bt) treatment. Results are presented as mean ± SEM. * $p<0.05$, compared to the control. (D) Total number of cells in mLNs of mice. (E) Percentage of CD4+T lymphocytes in mLNs of mice. (F) Percentage of Treg cells in mLNs of mice. (G) Representative dot plots of Tregs analysis. (H-J) Percentage of dendritic cells in mLNs of mice. (K) Representative dot plots of dendritic cells analysis. Gating strategies used for defining Tregs (L) and dendritic cells populations (M).

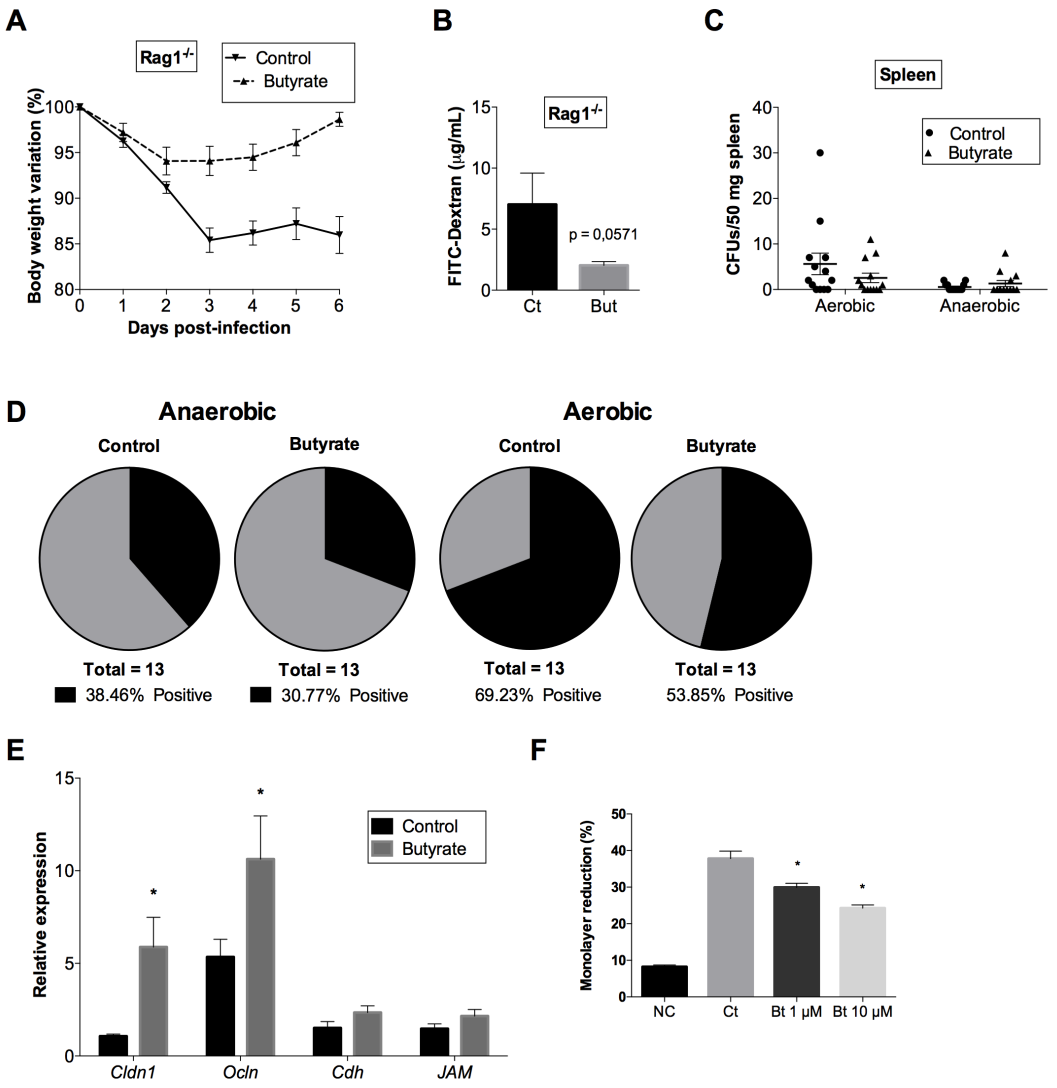

Figure S4. Protective effect of butyrate on infected mice, Related to Figures 3 and 4.
(A) Analysis of the body weight variation in *Rag1*-/- mice (n = 8). Results are presented as mean ± SEM. (B) Analysis of intestinal permeability by FITC-Dextran quantification in *Rag1*-/- mice 2 days post-infection (n = 3-4). Results are presented as mean ± SEM. * $p<0.05$, compared to the control. (C) Analysis of the bacterial translocation by counting the numbers of colonies after plating the spleen of mice previously treated with antibiotics and infected with *C. difficile* (n = 13). (D) Percentage of mice with bacterial translocation after colony growth of the spleen culture in anaerobic or aerobic condition at 37ºC (n = 13). Black = positive bacterial translocation, gray = negative bacterial translocation. (E) Analysis of gene expression by qPCR in mice on the 2nd day after infection with *C. difficile* (n = 5-9). Results were normalized by values obtained with samples from non-infected mice and are presented as mean ± SEM. * $p<0.05$, compared to the control. (F) Percentage of monolayer reduction 48 hours after culture with *C. difficile* supernatant and 10 µM butyrate. NC = negative control (cells without toxins or treatment), Ct = cells incubated with *C. difficile* supernatant for 48 hours; Bt = cells incubated with *C. difficile* supernatant and butyrate for 48 hours (n = 5-8). Results are presented as mean ± SEM. * $p<0.05$, compared to the negative control.

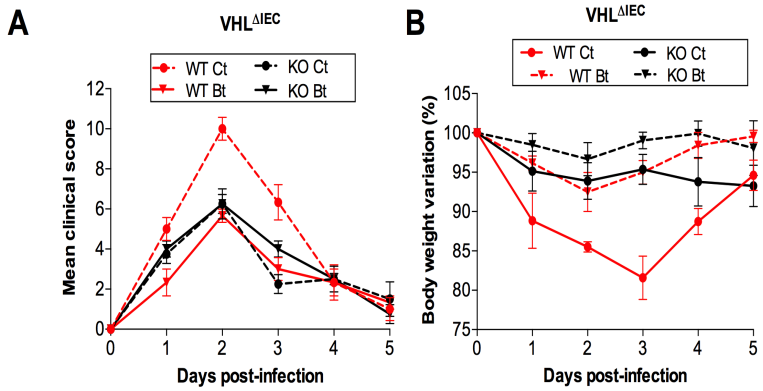

Figure S5. **Butyrate protection in CDI is dependent of HIF-1 stabilization, Related to Figure 5.** (A) Analysis of clinical score and (B) body weight variation of VhL-epithelium-specific knockout (KO) or wild-type (WT) infected mice treated or not with butyrate in drinking water (n = 3-4). Results are presented as mean ± SEM.

Supplementary tables.

Table S1. Clinical score (from Li *et al*., 2012), Related to STAR Methods.

Category	Scores*			
	0	**1**	**2**	**3**
Activity	Normal	Alert/Slow moving	Lethargic/Shaky	Inactive unless prodded
Posture	Normal	Back slanted	Hunched	Hunched/Nose down
Coat	Normal	Piloerection	Rough skin	Very ruffled/Puff/Ungroomed
Diarrhea	Normal	Soft stool/Discolored (yellowish)	Wet stained tail/ mucous +/- blood	Liquid/no stool (ileus)
Eyes/Nose	Normal	Squinted $^{1}/_{2}$ closed	Squinted/Discharge	Closed/Discharge

*Clinical score = sum of all parameters scores. Total possible score is 15.

Table S2. Primers used for qPCR, Related to STAR Methods.

Primer		Sequence (5' – 3')
Tumor necrosis factor *(Tnfa)*	sense	TCT TCT CAT TCC TGC TTG TGG C
	anti-sense	CAC TGG TGG TTT GCT ACG ACG
Interleukin-1beta (*Il1b*)	sense	GGC AGC TAC CTG TGT CTT TCC C
	anti-sense	ATA TGG GTC CGA CAG CAC GAG
Il6	sense	CTG CAA GAG ACT TCC ATC CAG
	anti-sense	AGT GGT ATA GAC AGG TCT GTT GG
Il10	sense	TGC CAA GCC TTA TCG GAA ATG
	anti-sense	AAA TCG ATG ACA GCG CCT CAG
Il12	sense	TGG TTT GCC ATC GTT TTG CTG
	anti-sense	ACA GGT GAG GTT CAC TGT TTC T
Il17	sense	TCA GCG TGT CCA AAC ACT GAG
	anti-sense	GAC TTT GAG GTT GAC CTT CAC AT
Il18	sense	CAG TGA ACC CCA GAC CAG AC
	anti-sense	AGG CGC ATG TGT GCT AAT CA
Il22	sense	AGA ATG TCA GAA GGC TGA AGG
	anti-sense	AGG AGC AGT TCT TCG TTT TCT AG
Transforming growth factor (*Tgfb*)	sense	CCG CAA CAA CGC CAT CTA TG
	anti-sense	CCC GAA TGT CTG ACG TAT TGA AG
Interferon-gamma *(Ifng)*	sense	ATG AAC GCA CAC ACT GCA TC
	anti-sense	CCA TCC TTT TGC CAG TTC CTC
Mieloperoxidase (*Mpo)*	sense	AGT TGT GCT GAG CTG TAT GGA
	anti-sense	CGG CTG CTT GAA GTA AAA CAG G
Cxcl1	sense	ACT GCA CCC AAA CCG AAG TC
	anti-sense	TGG GGA CAC CTT TTA GCA TCT T
Cxcl2	sense	GGG ACA AAT AGC TGC AGT CGG
	anti-sense	CTA CTC TCC TCG GTG CTT AC
Hypoxia inducible factor 1 (*Hif1a*)	sense	ATC TCG GCG AAG CAA AGA GTC
	anti-sense	TGG GGA AGT GGC AAC TGA T
Trefoil factor *3 (Tff3)*	sense	TGC AGA TTA CGT TGG CCT GT

	anti-sense	TGC AGA GGT TTG AAG CAC CA
Cathelicidin antimicrobial peptide *(Camp)*	sense	TCTCTACCGTCTCCTGGACCTG
	anti-esnse	CCACATACAGTCTCCTTCACT
6-phosphofructo-2-kinase/fructose-2,6-biphosphatase 3 (*Pfkfb3*)	sense	GGA GGT CGG CAT GTT GAA GA
	anti-sense	CTT TGG AAG GGC CTG AGA GG
Mucin-2 *(Muc2)*	sense	CGA CTG TGA GCA GTG TGT CA
	anti-sense	GGG TAG GGT CAC CTC CAT CT
Solute carrier family 2 (facilitated glucose transporter), member 1 *(Slc2a1)*	sense	CTT TGT GGC CTT CTT TGA AGT
	anti-sense	CCA CAC AGT TGC TCC ACA T
Forkhead box P3 *(FoxP3)*	sense	ACC ATT GGT TTA CTC GCA TGT
	anti-sense	TCC ACT CGC ACA AAG CAC TT
RAR-related orphan receptor gamma (*Rorc*)	sense	TCC ACT ACG GGG TTA TCA CCT
	anti-sense	AGT AGG CCA CAT TAC ACT GCT
Junction adhesion molecule (*JAM*)	sense	ACT GCT CAA TCT GAC GTC CA
	anti-sense	ATA GGG AGC TGT GAT CTG GC
Claudin-1 (*Cldn1*)	sense	CACTCCCAGACTCCACCACC
	anti-sense	CGATCCATCCCAGAGAAGCC
Occludin (*Ocln*)	sense	CTC TCA GCC AGC GTA CTC TT
	anti-sense	CTC CAT AGC CAC CTC CGT AG
Cadherin (*Cadh*)	sense	CCT GTC TTC AAC CCA AGC AC
	anti-sense	CAA CAA CGA ACT GCT GGT CA
Beta2-Microglobulin (*B2m*)	sense	CCC CAC TGA GAC TGA TAC ATA CG
	anti-sense	CGA TCC CAG TAG ACG GTC TTG
Human B2M	sense	GGA TCG GCG GCT CCA T
	anti-sense	CAT ACT CCT GCT TGC TGA TCC A
Human PFKFB3	sense	CCG AAG ATA AGG GGC ATA CC
	anti-sense	CAA GCT AAA ACC GTG AGT GAT T
Human VEGF	sense	ATC TTC AAG CCA TCC TGT GTG C
	anti-sense	CAA GGC CCA CAG GGA TTT TC
Human Slc2a1	sense	CAC CAC CTC ACT CCT GTT ACT TAC CT
	anti-sense	CAA GCA TTT CAA AAC CAT GTT TCT A
Human Claudin-1	sense	AGG TCT GGC GAC ATT AGT GG
	anti-sense	TGG TGT TGG GTA AGA GGT TG
Human occludin	sense	CAC GTT CGA CCA ATG C
	anti-sense	CCC GTT CCA TAG GCT C
Primers V3-V4	sense	TCGTCGGCAGCGTCAGATGTGTATAAGAGACA GCCTACGGGNGGCWGCG
	anti-sense	GTCTCGTGGGCTCGGAGATGTGTATAAGAGAC AGGACTACHVGGGTATCTAATCC
16S of Eubacteria	sense	ACT CCT ACG GGA GGC AGC AGT
	anti-sense	ATT ACC GCG GCT GCT GGC

Table S3. Histological score, Related to STAR Methods..

Category		0 (none)	1 (mild)	2 (moderate)	3 (severe)
Mucosal epithelium	Ulceration	None	Mild surface	Moderate	Extensive full thickness
Crypts	Mitotic Activity	Lower third	Mild mid third	Moderate mil third	Upper third
	Mucus depletion	None	Mild	Moderate	severe
Lamina propria	Mononuclear infiltrate	None	Mild	Moderate	severe
	Granulocyte infiltrate	None	Mild	Moderate	severe
	Vascularity	None	Mild	Moderate	severe
	Fibrin deposition	None	Mucosal	Submucosal	transmural
Submucosal	Mononuclear infiltrate	None	Mild	Moderate	severe
	Granulocyte infiltrate	None	Mild	Moderate	severe
	Edema	None	Mild	Moderate	severe